General Disclaimer

One or more of the Following Statements may affect this Document

- This document has been reproduced from the best copy furnished by the organizational source. It is being released in the interest of making available as much information as possible.

- This document may contain data, which exceeds the sheet parameters. It was furnished in this condition by the organizational source and is the best copy available.

- This document may contain tone-on-tone or color graphs, charts and/or pictures, which have been reproduced in black and white.

- This document is paginated as submitted by the original source.

- Portions of this document are not fully legible due to the historical nature of some of the material. However, it is the best reproduction available from the original submission.

Produced by the NASA Center for Aerospace Information (CASI)

NASA CR-134504

(NASA-CR-134504) FLOW IN A POROUS NOZZLE WITH MASSIVE WALL INJECTION (Arizona Univ., Tucson.) 69 p HC $5.50 CSCL 20D
N74-12082
Unclas
G3/12 23314

FLOW IN A POROUS NOZZLE WITH MASSIVE WALL INJECTION

by

R. B. Kinney, Z. Cielak, H. C. Perkins

AEROSPACE AND MECHANICAL ENGINEERING DEPARTMENT

UNIVERSITY OF ARIZONA
TUCSON, ARIZONA

prepared for

NATIONAL AERONAUTICS AND SPACE ADMINISTRATION

NASA Lewis Research Center
Grant NGR 03-002-213

August, 1973

NASA CR-134504

FLOW IN A POROUS NOZZLE WITH MASSIVE WALL INJECTION

by

R. B. Kinney, Z. Cielak, H. C. Perkins

AEROSPACE AND MECHANICAL
ENGINEERING DEPARTMENT

UNIVERSITY OF ARIZONA
TUCSON, ARIZONA

prepared for

NATIONAL AERONAUTICS AND SPACE ADMINISTRATION

NASA Lewis Research Center
Grant NGR 03-002-213

August, 1973

FOREWORD

This report, one of a series of four, describes analytical and experimental results for flow in a convergent-divergent nozzle with massive wall blowing. The work was supported by the Nuclear Systems Division, NASA Lewis Research Center, under Grant NGR 03-002-213. Mr. Albert F. Kascak was the technical manager.

PRECEDING PAGE BLANK NOT FILMED

TABLE OF CONTENTS

PRECEDING PAGE BLANK NOT FILMED

SUMMARY

An analytical and experimental investigation has been conducted to determine the effect of massive wall injection on the flow characteristics in a nozzle. The experiments were performed on a water table with a porous-nozzle test section. This had 45° and 15° half angles of convergence and divergence, respectively, throat radius of 2.5 inches, and throat width of 3 inches. The hydraulic analogy was employed to qualitatively extend the results to a compressible gas flow through the nozzle.

An analysis of the water-table flow was made using a one-dimensional flow assumption in the continuity and momentum equations. Allowance was made for fluid injection along the nozzle wall. Predictions of the flow conditions in the nozzle were made for injection rates up to 30% of the inlet flow rate.

Experimental results from the water table include contours of constant Froude and Mach number with and without wall injection. Photographs of the visualized flow showing the injected layer are also presented for a range of injection rates.

An analysis of a compressible flow in a nozzle was made in a manner analogous to that for the water flow. It is shown that the effect of blowing is to move the sonic position downstream of the geometric throat. Similar results were determined for the incompressible water-table flow.

Limited photographic results are also presented for the injection of air, CO_2, and Freon-12 into a main-stream air flow in a convergent-divergent nozzle. Schlieren photographs were used to visualize the flow, and qualitative agreement between the results from the gas tunnel and the water table is good.

All the results are discussed in detail. Conclusions are presented which should be an aid in the preliminary design of a rocket nozzle for use in the gas core nuclear rocket.

INTRODUCTION

Advanced rocket engines, in particular the gas core nuclear rocket, are expected to produce gas temperatures at the entrance to the nozzle in the neighborhood of 20,000°K (1). Such temperatures are orders of magnitude above those which can be tolerated by the structural components of the nozzle fabricated from existing materials. Therefore, the nozzle wall must be thermally protected to a much higher degree than that required by the current generation of rocket nozzles.

A major portion of the nozzle heating is due to the thermal radiation from the high temperature gases in the nozzle and nuclear reactor core. This contribution can be diminished by creating an optically thick protective fluid layer enveloping the hot core gases as they expand through the nozzle. This protective fluid layer must exist adjacent to the nozzle wall and may be formed by injection of a suitable cooling fluid through the wall. In addition to providing a radiation shield, the injected fluid must also diminish the convective heat transfer through the mechanism of transpiration cooling.

To facilitate injection of the coolant fluid, the nozzle can be fabricated from a porous material. It is expected that injection on the order of 10 to 20 percent of the main stream mass flow may be required to provide convective and radiation protection. In view of this large amount of injection, the changes in the flow-field characteristics due to injection need to be investigated.

To the authors' knowledge, very little information is available on flow systems utilizing such high injection flow rates through a porous wall. The bulk of the existing work applies to boundary layer flows in which the injection velocities are less than one percent of those in the external flow. These prior studies have been further limited to flows with small streamwise pressure gradients. Therefore, they do not apply directly to internal flows with large streamwise gradients in pressure and density, such as are found in supersonic nozzles.

In the present report, an experimental approach is adopted for the study of nozzle flows with large wall-

transpiration rates. Based on the hydraulic analogy, a compressible gas flow is modeled with a water flow having a free surface. In its simplest form, the analogy applies between one-dimensional, open-channel liquid flow and isentropic, one-dimensional, internal gas flow. The flow variables in one-dimensional open-channel flow are local height and Froude number. They vary in the flow direction which is perpendicular to local gravitational acceleration. The local height and Froude number may be related to an equivalent local pressure and Mach number in an isentropic, one-dimensional nozzle gas flow. The analogy is exact for a perfect gas with a specific heat ratio γ of 2. If the channel width-ratio (local width to throat width) is set equal to the nozzle area ratio (local area to throat area), the Froude number is equal to the Mach number, and the square of the height-ratio (local to stagnation) is equal to pressure ratio (local to stagnation). Once the Mach number or pressure ratio is found in this manner, the other properties may be found directly from the isentropic tables. For gases with different γ, appropriate correction factors exist (2). Previous reports in this series have described the analogy in more detail (3,4).

The hydraulic analogy does not directly apply to a flow with injection. Nevertheless, it is useful in a qualitative analysis of this type of flow. Such an analysis is performed here. It is simplified due to the assumption of inviscid and uniform flow. That is, the effects of viscosity and the flow variation across the nozzle are neglected. At any cross-section the flow has plug-flow characteristics with constant liquid height in the transverse direction.

In the sections to follow, the emphasis is placed on studying the (a) Froude (Mach) number distribution, (b) shifting of the hydrodynamic throat (position where F and M = 1), and (c) thickness of the injected fluid layer, all as functions of the injection rate. The calculated results for one-dimensional flow are compared with experimental data obtained on the water table. Results presented here are for injection through a uniformly porous wall. Results for injection through a wall with discrete slots are presented in a subsequent report.

Some results are also presented for injection of different gases (air, CO_2, Freon-12) into the transonic region of a plane porous nozzle operating with air as the main flow. The qualitative agreement between the

incompressible water table results and those obtained in the wind tunnel is good.

It should be re-emphasized that the primary objective of this work is to determine general changes in the flow-field characteristics caused by high rates of wall injection, and not the precise prediction of the flow field. Therefore, the analytical results are used only as an aid in interpreting the experimental findings.

HYDRAULIC ANALOGY

The hydraulic analogy was first discussed in detail in Preiswerk (5,6). Loh (7) has reprinted much of this earlier work and has extended the analogy to the case of unsteady flow. In the analogy, an assumption is made that accelerations in the vertical direction are negligible. To approximately meet this assumption, it is necessary to operate the water table with modest stagnation heights in the upstream region where the velocity approaches zero. For the porous wall nozzle, this is difficult since one must have sufficient height in the supercritical region after the throat for controlled blowing to be visualized. Thus with injection, it is necessary to operate with stagnation heights on the order of 2.5 to 3 inches instead of the more desirable 1 to 1.5 inches.

To investigate the effect of stagnation height on the distribution of Froude number in a nozzle, a series of test were made with gradually decreasing stagnation heights. These results are shown in Figure 1.

The Froude number is analogous to the Mach number in compressible isentropic gas flows. These data were obtained without injection through the nozzle wall, the contour of which is shown in the figure. This nozzle has a 45° inlet half angle and a 15° half angle in the downstream section.

As expected, the results with different stagnation heights become essentially indistinguishable as H_o approaches one inch. These results indicate that vertical acceleration effects are important for stagnation water depths greater than approximately 1.5 inches. Preiswerk has found similar results for an impermeable-walled nozzle.

Figure 2 shows these same results plotted in terms of Mach number for an equivalent gas with $\gamma = 1.4$. Reference (4) has indicated the procedure by which the Froude number results (Froude corresponds to the Mach number in a gas with $\gamma = 2$) can be corrected to give Mach number results for other values of γ.

Briefly the correction follows from equating the area ratio formula for the compressible-gas flow to the width-

ratio result for water-table flow. These are:

$$\frac{A}{A_{th}} = \frac{1}{M}\left[\left(\frac{2}{\gamma+1}\right)\left(1 + \frac{\gamma-1}{2} M^2\right)\right]^{(\gamma+1)/2(\gamma-1)} \qquad (1)$$

and

$$\frac{B}{B_{th}} = \frac{1}{F}\left[\left(\frac{2}{3}\right)\left(1 + \frac{F^2}{2}\right)\right]^{3/2} \qquad (2)$$

One can quickly see that in the analogy, F corresponds to M when $\gamma = 2$ for the analogous gas.

If one equates these two expressions, a single equation results which can be solved using specified values of γ and F. The value of M so obtained is called the "corrected Froude number" and it is this value which is shown in Figure 2. Details for obtaining the correction are given in (4). Cuffel et. al. (8) have obtained Mach number distributions in an axisymmetric nozzle having convergence and divergence half-angles of 45° and 15°, respectively. The centerline Froude numbers from the water table, corrected to $\gamma = 1.4$, show excellent agreement with the Mach number results from (8) (see Reference 4, Figure 7). It is worth noting that the good agreement was obtained even with a stagnation height of 2.8 inches on the water table. Thus, we may conclude that for th case of no-injection, excellent agreement occurs between the incompressible open-channel flow and compressible flow in an axisymmetric nozzle.

The question now arises as to whether or not the analogy can be applied to the nozzle flow with wall-injection. To answer this, one must first obtain the governing equations for flow on the water-table and flow of a compressible gas. These equations are well known for the case of flow through impermeable-walled nozzles. However, they have yet to be derived for the case where fluid is injected from the nozzle wall into the main stream flow. The derivation of the water-table equations will be presented in this first section. The next section contains the derivation of the gas-flow equations, following which the basis for the analogy is discussed.

ANALYSIS OF WATER-TABLE FLOW WITH INJECTION

Derivation of Equations

The analytical approach taken here is similar to that adopted for the no-injection case. That is, the principles of mass continuity and flow momentum constitute the essential basis for the analysis. As in the no-injection case, the characteristic parameter for the open-channel liquid flow with injection is Froude number. However, an additional parameter must be introduced for the injected fluid. This is the wall Froude number, F_W, which is defined as the ratio of the injection velocity and $(gH)^{1/2}$, where H is the local liquid height in the channel, and g is the local gravitational acceleration. Recall that Froude number, F, is defined in the same manner, with the injection velocity replaced by local main fluid flow velocity.

The injection is normal to the wall and encompasses the entire height of the area wetted by the main stream. That is, the injected fluid is always in contact with the main stream flow, and never above it. The flow is assumed to be steady, inviscid, incompressible, free of surface tension, with a hydrostatic pressure distribution and uniform velocity at any cross section. For simplicity, the flow will be taken to be one-dimensional.

Figure 3 depicts the flow boundaries and the elemental control volume. The following terminology is used:

V - flow velocity in x-direction

v_w - injection velocity

ρ - fluid density

P - hydrostatic pressure

H - liquid height in the channel

B - channel width

θ - channel wall angle

The continuity equation can be expressed in the simple form,

$$d(\rho VHB) = \frac{2\rho_w v_w H\, dx}{\cos\theta} \qquad (3)$$

where the term on the left hand side is the mass flow-rate differential between downstream and upstream control surfaces in the main-stream fluid, while the right-hand side expresses the total flow rate injected into the control volume (from both sides of the channel). In Equation (3) all of the variables, including v_w, may be only a function of x, the flow direction.

The contributing factors to the x-momentum are:

i) Momentum of the main stream fluid flowing into the control volume, namely $\dot{m}V$ or $\rho V^2 HB$.

ii) x-component of the momentum of the injected fluid

$$2\rho_w v_w\left[\frac{2H+dH}{2}\ \frac{dB}{2\sin\theta}\right]v_w \sin\theta = \rho_w v_w^2 H\, dB$$

where the bracketed term is the injection area per wall.

iii) Momentum outflow, given by the first two terms of the Taylor series expansion about the x-location corresponding to the upstream control surface. This is

$$\rho V^2 HB + d(\rho V^2 HB).$$

Thus, the total increase in x-momentum of the flow coming out of the control volume, that is, the difference between the outflow and inflow momentums, becomes

$$d(\rho V^2 HB) - \rho_w v_w^2 H\, dB$$

Since we have assumed inviscid flow, the net force acting

on the control volume is the change of the hydrostatic pressure force due to the fluid height change; that is,

$$- \rho g B H \, dH.$$

This is a positive quantity since H decreases in the x-direction. Thus, the momentum equation in its entirety, becomes

$$- \rho g B H \, dH = d(\rho V^2 H B) - \rho_w v_w^2 H \, dB$$

This also may be written as

$$- \rho g B H \frac{dH}{dx} = \rho V H B \frac{dV}{dx} + V \frac{d}{dx}(\rho V H B) - \rho_w v_w^2 H \frac{dB}{dx}$$

From the continuity relation, the second term on the right hand side of the above equation is

$$2\rho_w v_w V H / \cos \theta$$

Also from continuity,

$$\frac{dV}{dx} = - V \left[\frac{1}{H} \frac{dH}{dx} + \frac{1}{B} \frac{dB}{dx} \right] + \frac{2\rho_w v_w}{\rho B \cos \theta}$$

Here we have noted that $d\rho/dx = 0$ since the main stream fluid is taken to be incompressible.

From the channel geometry,

$$dB/dx = 2 \tan \theta$$

With the above identities, the momentum equation reduces to

$$\left(1 - \frac{V^2}{gH}\right) \frac{dH}{dx} = \frac{H}{B}\left[2 \frac{V^2 + (\rho_w/\rho)v_w^2}{gH} \tan\theta - \frac{4(\rho_w/\rho)v_w V}{gH \cos\theta}\right] \qquad (4)$$

As previously stated, the ratio of the liquid velocity V to the propagation speed of a weak surface wave, $\sqrt{gH}$, is known as the Froude number, F. Flow is classified as subcritical, critical, or supercritical when F is respectively less than, equal to, or greater than unity. The ratio $v_w/\sqrt{gH}$ is the wall Froude number and is given the symbol F_w.

Introducing F and F_w into Equation (4) and noting that on the water table $\rho_w = \rho$, one obtains

$$\frac{dH}{dx} = \frac{2}{1-F^2} \frac{H}{B\cos\theta}\left[(F^2 + F_w^2) \sin\theta - 2FF_w\right] \qquad (5)$$

Equation (5) represents the variation of the liquid height in the channel including the effects of blowing.

The variation of the Froude number with x location is found by combining the continuity relation written as

$$HB \frac{dV}{dx} + VH \frac{dB}{dx} + VB \frac{dH}{dx} = \frac{2v_w H}{\cos\theta}$$

with the expression

$$\frac{dV}{dx} = \frac{V}{F} \frac{dF}{dx} + \frac{V}{2H} \frac{dH}{dx}$$

This is obtained by differentiating

$$V = F\sqrt{gH}$$

The relation for dB/dx previously stated is also used. The final equation representing the Froude number distribution is

$$\frac{dF}{dx} = -\frac{3}{2}\frac{F}{H}\frac{dH}{dx} + \frac{2}{B\cos\theta}(F_w - F\sin\theta) \qquad (6)$$

Equations (5) and (6) are coupled nonlinear first order differential equations. For a given nozzle geometry they can be integrated numerically to find the Froude number and liquid height variations as a function of x, the flow direction.

It is now of interest to examine the general flow characteristics revealed by the equations derived above. This will be taken up next, following which the corresponding gas-flow equations will be derived.

Flow Characteristics

First consider the flow without injection, $F_w = 0$. Equations (5) and (6) reduce to:

$$\frac{dH}{dx} = \frac{2F^2}{1-F^2}\frac{H}{B}\tan\theta \qquad (7)$$

$$\frac{dF}{dx} = \left(\frac{F^2+2}{F^2-1}\right)\frac{F}{B}\tan\theta \qquad (8)$$

At critical flow ($F = 1$), the gradient in water height, dH/dx, must be continuous. This is analogous to the condition that the pressure gradient be continuous at $M = 1$ in gas flows. Consequently, $F = 1$ must correspond to $\theta = 0$, since otherwise the numerator of Equation (7) would not be zero. Recalling that θ is the local slope of the nozzle contour (measured from the axis), it is seen that $\theta = 0$ represents the position of the geometrical throat. It can be seen from Equation (8) that dF/dx is also continuous at $F = 1$.

Assume now that the subcritical region is upstream of the throat; here by definition, $F < 1$ and $\theta < 0$ as indicated in Figure 3. From the Equations (7) and (8), in this

region $dH/dx < 0$ and $dF/dx > 0$. Consequently the flow must accelerate with diminishing height level toward the throat. Downstream of the throat, $\theta > 0$. If, in addition, $dH/dx < 0$, then $dF/dx > 0$. On the other hand, if $dH/dx > 0$, then $dF/dx < 0$. Thus, for continually decreasing liquid height in the convergent-divergent channel, the flow must be accelerated to supercritical conditions ($F > 1$). We shall deal here with this category of flow. It is possible, however, to decelerate the flow after it has reached critical conditions at the throat. This would be important in the analysis of diffusers.

In a similar manner, we may arrive at the hydrodynamic throat conditions for the flow with injection. Here, the (shock free) critical flow position may be found from Equation (5) assuming dH/dx to be finite for $F = 1$. Then the term in brackets must vanish. That is, when $F = 1$,

$$(1 + F_{w,t}^2) \sin \theta_t - 2 F_{w,t} = 0 \qquad (9)$$

Here $F_{w,t}$ refers to the wall Froude number at the hydrodynamic throat, and θ_t to the corresponding wall angle. The angle θ_t is bounded by $\pm\pi/2$, and $\sin \theta_t$ is required to be positive for Equation (9) to hold (i.e. $F_{w,t}$ cannot be negative). Thus, θ_t must be positive. This means that the hydrodynamic throat ($F = 1$), for the case of wall injection, appears in the divergent portion of the nozzle, downstream of the geometric throat.

The solution to Equation (9) is $F_{w,t} = (1 \pm \cos \theta_t)/(\sin \theta_t)$. For the nozzle under consideration the maximum value of θ_t is 15°. The corresponding values of $F_{w,t}$ satisfying the Equation (9) are 0.131 and 7.59. The wall Froude number of 7.59 appears to be unrealistic since an injected fluid velocity of more than seven-fold the main stream velocity would totally disrupt the flow. Furthermore, as θ_t approaches zero, the upper values of the wall Froude number get arbitrarily large. Thus, only the lower values of the wall Froude number, given by

$$F_{w,t} = \frac{1-\cos \theta_t}{\sin \theta_t} \qquad (10)$$

appear to have physical significance.

At F_W equal to $F_{W,t}$ the expression for $(dH/dx)_t$ becomes indeterminant. However, its value may be determined with the aid of l'Hôpital's rule. One finds

$$\left(\frac{dH}{dx}\right)_t = \lim_{\substack{x\to x_t \\ \theta\to\theta_t \\ F\to 1}} \frac{2H\{(2F(dF/dx) + 2F_W(dF_W/dx))\sin\theta\}}{-2FB\cos\theta\,(dF/dx)} +$$

$$\frac{2H\{(F^2 + F_W^2)\cos\theta(d\theta/dx)\}}{-2FB\cos\theta\,(dF/dx)} -$$

$$\frac{2H\{2[F(dF_W/dx) + F_W(dF/dx)]\}}{-2FB\cos\theta\,(dF/dx)} \qquad (11)$$

If the wall injection velocity is constant with x, then

$$\frac{dF_W}{dx} = -\frac{1}{2}\frac{F_W}{H}\frac{dH}{dx}$$

When this is inserted into Equation (11) together with Equation (6) defining dF/dx, one obtains a quadratic equation in dH/dx. The final solution, after taking the limit and considerable algebra, is

$$\left(\frac{dH}{dx}\right)_t = \frac{H}{3B\cos\theta}\{(6F_W - 5\sin\theta - F_W^2\sin\theta) \pm$$

$$[(6F_W - 5\sin\theta - F_W^2\sin\theta)^2 +$$

$$6((1 + F_W^2)\,B\cos^2\theta\,(d\theta/dx) -$$

$$4(F_W - \sin\theta)^2)]^{1/2}\}$$

with all variables being evaluated at the hydrodynamic throat.

In the throat region the channel wall has a circular

shape of radius R. Thus

$$\frac{d\theta}{dx} = \frac{1}{R \cos \theta}$$

For $F_{w,t}$ given by Equation (10) the expression for the slope of the liquid-height further reduces to

$$\left(\frac{dH}{dx}\right)_t = -\frac{4H(1 - \cos \theta)}{3B \sin \theta} \{1 \pm [1 + \frac{3}{4}(\frac{B}{R \cos \theta (1-\cos \theta)} - 2)]^{1/2}\} \quad (12)$$

The positive sign will be chosen to render the value $(dH/dx)_t < 0$, since for small θ and B of the same order as R the second term under the radical sign is positive.

Equations (5), (6), and (12) together with the known nozzle geometry yield sufficient information for numerical studies of the Froude number and the liquid height variations along the nozzle. In addition, the thickness of the injected layer measured normal to the wall, δ, may be estimated using the simple expression

$$\delta(x) = \frac{\text{total mass injected upstream of the x position}}{(2\rho HV/\cos \theta)} \quad (13)$$

This assumes that the injected fluid displaces the main flow adjacent tc the wall without mixing with the free-stream flow. This expression follows from the continuity equation for the incompressible injected fluid. In keeping with the one-dimensional idealization, the fluid in the injected layer is assumed to have the same velocity, V, as that in the main flow.

Results of calculations using these equations will be presented shortly.

ANALYSIS OF COMPRESSIBLE-GAS FLOW WITH INJECTION

Derivation of Equations

Let us now look at the problem of a plane porous nozzle with a compressible fluid injected through the wall into a compressible main scream fluid.

Our model will assume the following:

1. inviscid flow.
2. injection normal to the nozzle wall.
3. perfect gas behavior (or $Pv = ZRT$ can be used).
4. a plane porous nozzle with injection only through two opposite sides.
5. unit depth normal to the plane of flow, i.e. $H = 1$.

The continuity equation then becomes (see Figure 3 for the geometry)

$$\frac{2\rho_w V_w}{\cos\theta} = \frac{d}{dx}(\rho V B) \tag{14}$$

The momentum equation can be developed in a manner similar to the incompressible case. We have

$$\sum F_x = \text{Rate of Creation of Momentum}$$

In the absence of shear:

$$\sum F_x = -B\,dP$$

The momentum flow into the control volume is $\rho V^2 B$ plus the X-momentum brought in with the injected fluid. This latter quantity is

$$(m_{inj})_{in} = (\rho_w v_w \, dx/\cos\theta) v_w \sin\theta$$

Since $(dx/\cos\theta)(\sin\theta) = dB/2$, we have

$$(m_{inj})_{in} = \rho_w v_w^2 \, dB/2$$

The complete momentum and force balance then becomes (injection through two sides)

$$-B \, dP = \frac{d}{dx} (\rho V^2 B) dx - \rho_w v_w^2 \, dB$$

In differential form we have (note $dB = 2 \, dx \tan\theta$)

$$\frac{dP}{dx} = \frac{2\rho_w v_w^2}{B} \tan\theta - \frac{1}{B} (\rho V B) \frac{dV}{dx} - \frac{V}{B} \frac{d}{dx} (\rho V B) \quad (15)$$

Substituting for the last term from the continuity equation we find:

$$\frac{dP}{dx} = \frac{2\rho_w v_w}{B} \left(v_w \tan\theta - \frac{V}{\cos\theta}\right) - \rho V \frac{dV}{dx} \quad (16)$$

The energy equation can be developed in a similar manner. Since

$$E_{in} = E_{out}$$

and

$$E_{in} = \rho VB(V^2/2 + h) + \frac{2\rho_w v_w dx}{\cos\theta}(v_w^2/2 + h_w)$$

$$E_{out} = \rho VB(V^2/2 + h) + \frac{d}{dx}[\rho VB(V^2/2 + h)]\, dx$$

one obtains,

$$\frac{2\rho_w v_w}{\cos\theta}[(v_w^2/2) + h_w] = \frac{d}{dx}[\rho VB(V^2/2 + h)] \qquad (17)$$

We can now manipulate these equations, using also the perfect gas equation, to find a relation for dT/dx. In a manner similar to that used for Equation (5) the effect of injection on the location of the hydrodynamic throat can then be determined.

Combining the energy and continuity equations and assuming that $c_{p,w} = c_p$ we have

$$\frac{2\rho_w v_w}{\cos\theta}\left[\frac{v_w^2 - V^2}{2} + c_p(T_w - T)\right] = \rho VB\left[V\frac{dV}{dx} + c_p\frac{dT}{dx}\right] \qquad (18)$$

From continuity

$$\rho B\frac{dV}{dx} + \rho V\frac{dB}{dx} + VB\frac{d\rho}{dx} = \frac{2\rho_w v_w}{\cos\theta} \qquad (19)$$

The perfect gas relation can be differentiated to give

$$\frac{d\rho}{dx} = \frac{1}{RT}\frac{dP}{dx} - \frac{\rho}{T}\frac{dT}{dx} \qquad (20)$$

Substituting the momentum equation for dP/dx, one finds $d\rho/dx$ in terms of dT/dx and dV/dx. This expression is then substituted into Equation (19) to find dV/dx. Noting

that $dB/dx = 2 \tan \theta$ we have

$$\frac{dV}{dx} = \frac{2\rho_w v_w}{\rho B \cos \theta} - \frac{2V \tan \theta}{B} + \frac{V}{\rho}\frac{\rho}{T}\frac{dT}{dx} -$$

$$\frac{V}{\rho RT}\frac{2\rho_w v_w}{B}[v_w \tan \theta - V/\cos \theta] + \frac{V^2}{RT}\frac{dV}{dx}$$

or

$$\frac{dV}{dx}\left[1 - \frac{V^2}{RT}\right] = \frac{2\rho_w v_w}{\rho B \cos \theta} - \frac{2V \tan \theta}{B} + \frac{V}{T}\frac{dT}{dx} -$$

$$\frac{2\rho_w v_w V}{\rho RTB}[v_w \tan \theta - V/\cos \theta] \qquad (21)$$

Now substituting this expression into the energy equation, Equation (18), we find

$$\frac{dT}{dx}\left[\rho V B c_p + \frac{\rho V^2 B V}{T(1-V^2/RT)}\right] = \frac{2\rho_w v_w}{\cos \theta}\left[\frac{v_w^2 - V^2}{2} + c_p(T_w - T)\right]$$

$$- \frac{\rho V^2 B}{(1-V^2/RT)}\left[\frac{2\rho_w v_w}{\rho B \cos \theta} - \frac{2V \tan \theta}{B}\right]$$

$$+ \frac{\rho V^2 B 2\rho_w v_w V}{\rho RTB(1-V^2/RT)}[v_w \tan \theta - V/\cos \theta] \qquad (22)$$

Using

$$M^2 = V^2/\gamma RT$$

and

$$M_w^2 = v_w^2/\gamma RT$$

(note M_w is defined on T, not T_w) we can reduce this

equation to some extent. For example, the bracketed term on the left hand side becomes

$$\rho VB\left[\frac{c_p(1-M^2)}{(1-\gamma M^2)}\right]$$

Using this, an intermediate result is

$$\frac{dT}{dx} = \frac{(1-\gamma M^2)}{c_p(1-M^2)}\left\{\frac{2\rho_w v_w}{\rho VB\cos\theta}\left[\frac{\gamma RT}{2}(M_w^2 - M^2) + Tc_p\left(\frac{T_w}{T}-1\right)\right] - \frac{2\rho_w v_w}{\rho VB\cos\theta}\frac{V^2}{(1-V^2/RT)}(1 + \gamma M^2 - \gamma M M_w \sin\theta) + \frac{2V^2\tan\theta}{B(1-V^2/RT)}\right\} \quad (23)$$

Further manipulation results in the final equation (note $\gamma R/c_p = (\gamma-1)$):

$$\frac{dT}{dx} = \frac{2(\gamma-1)T}{(1-M^2)B}\left\{\frac{(1-\gamma M^2)\rho_w v_w}{\rho V\cos\theta}\left[\frac{M_w^2-M^2}{2} + \frac{(T_w/T-1)}{(\gamma-1)}\right] - \frac{\rho_w v_w M^2}{\rho V\cos\theta}(1 + \gamma M^2 - \gamma M M_w \sin\theta) + M^2\tan\theta\right\} \quad (24)$$

This rather complicated expression is the counterpart to Equation (5) obtained for the water-table flow. An expression for dM/dx could also be obtained with steps similar to those used to obtain Equation (6).

Flow Characteristics

At the hydrodynamic throat, M = 1. In order for dT/dx to be continuous there, the term in braces must approach a limit of zero. We then have, with M = 1,

$$\sin\theta_t - \frac{\rho_w}{\rho}M_{w,t}(1+\gamma-\gamma M_{w,t}\sin\theta_t) + \left[\frac{(T_w/T-1)}{(\gamma-1)} + \frac{M_{w,t}^2-1}{2}\right]\left[\frac{\rho_w}{\rho}M_{w,t}(1-\gamma)\right] = 0$$

Expanding, one obtains the cubic equation,

$$M_{W,t}^3 + \frac{2\gamma}{1-\gamma} M_{W,t}^2 \sin\theta_t - \left[\frac{(\gamma+3)}{(1-\gamma)} + \frac{2(T_W/T-1)}{(1-\gamma)}\right] M_{W,t} + \frac{2p}{\rho_W(1-\gamma)} \sin\theta_t = 0 \qquad (25)$$

Solving the cubic for $M_{W,t}$ as a function of θ_t will reveal the location where $M = 1$ in the nozzle. A similar situation arose in connection with $F_{W,t}$ and θ_t when $F = 1$. However, in that case a quadratic equation resulted for $F_{W,t}$.

Solution to the Cubic Equation

Consider the equation

$$x^3 + a_1 x^2 + a_2 x + a_3 = 0$$

If we let

$$Q = \frac{3a_2 - a_1^2}{9} \quad ; \qquad R = \frac{9a_1a_2 - 27a_3 - 2a_1^3}{54}$$

then if $D = Q^3 + R^2$, we have the following possibilities:

(a) one real root and two complex conjugate roots if $D > 0$.

(b) all real roots (and at least two are equal) if $D = 0$.

(c) all roots real and unequal if $D < 0$.

From our equation

$$a_1 = \frac{2\gamma}{1-\gamma} \sin\theta_t$$

$$a_2 = -\left[\frac{(\gamma+3)+2(T_W/T-1)}{1-\gamma}\right]$$

$$a_3 = \frac{2\sin\theta_t}{1-\gamma}\frac{\rho}{\rho_W}$$

It becomes algebraically cumbersome to develop expressions for Q^3 and R^2, so we shall look at a_1, a_2, and a_3, directly. Since for compressible fluid, $\gamma > 1$, and we are interested in $0 \leq \theta_t \leq \pi/2$, we have $a_1 \leq 0$. For a_2, all cases of interest will have $T_W/T \leq 1$. Note that $(\gamma+3) > 0$, and in particular $|(\gamma+3)| \geq |2(T_W/T-1)|$. Since $(1-\gamma) < 0$, the numerator is positive and the denominator is negative. Therefore, $a_2 > 0$. Concerning a_3, we see that $a_3 \leq 0$.

In summary, a_1 and a_3 are negative and a_2 is positive. Since $Q = (3a_2-a_1^2)/9$ it can be either positive or negative. Therefore we must look at the magnitudes of the terms to establish the sign of Q and also of R.

Let $\theta_t = 10°$, then for $\gamma = 1.4$ we have

$$a_1 = \frac{2\gamma}{1-\gamma}\sin\theta_t = -(7)(0.173) = -1.2$$

For $T_W << T$ we have

$$a_2 = -\left[\frac{\gamma+3-2}{1-\gamma}\right] = 6$$

So in order of magnitude

$$Q = \frac{3a_2-a_1^2}{9} = \frac{1}{9}(18 - 1.4) = 1.85$$

or $Q > 0$.

Now, the sign of R can be established by looking at a_3. We have

$$a_3 = \frac{2\sin\theta_t}{(1-\gamma)}\frac{\rho}{\rho_W} < 0$$

For a perfect gas $\rho/\rho_W = T_W/T^*$ So for an actual rocket nozzle $\rho/\rho_W < 1$. We shall pick, rather arbitrarily, $\rho/\rho_W = 1/4$. Then

$$a_3 = \frac{(2)(0.173)}{(-.5)}(.25) = -0.173$$

and

$$R = \frac{9(-1.2)(6)-27(-.17)-2(-1.2)^3}{54}$$

or

$$R = \frac{-56.4}{54} \simeq -1$$

Thus $R < 0$. Careful consideration of the possible range that the variables can take indicates that it is generally true that $R < 0$. Recalling that $D = Q^3 + R^2$, and since $Q^3 > 0$ and $R^2 > 0$, we have $D > 0$. Therefore, one root is real and two are complex conjugates. Determining the one real root will establish the location for $M = 1$.

Because there are a large number of parameters involved, the solution for $M_{W,t}$ will be obtained for selected values for T/T_W, ρ/ρ_W and γ. The equation will be solved for the one real root to determine the $M_{W,t}$ value as a function of θ_t.

The solution is presented in Table I. The geometry is noted in Figure 4. The procedure involves picking values of $\sin\theta_t$ and obtaining $M_{W,t}$ by successive trials. Thus for $T_W/T = \rho/\rho_W = 1.0$ and $\gamma = 1.4$, we find that a value of $M_W = 0.090$ will produce $M = 1$ at $\theta_t = 11°20'$. This angle is measured counterclockwise from the geometric throat (where $\theta = 0$). The effect of injection is therefore to cause the hydrodynamic throat to move downstream from the location of A* associated with the geometry, (i.e. for non-porous nozzles, $M = 1$ when $A = A^*$).

---

*This assumes that the injectant gas is the same as the propellant gas, for example hydrogen, and enters the nozzle at the local static pressure.

TABLE I LOCATION OF M = 1 WITH INJECTION

M_w	θ_t	$\sin \theta_t$
$T_w/T = 1.0$, $\rho/\rho_w = 1.0$, $\gamma = 1.4$.		
0.045	5° 45'	0.100
0.090	11° 20'	0.200
0.130	17° 28'	0.300
$T_w/T = 1/2$, $\rho/\rho_w = 1/2$, $\gamma = 1.4$.		
0.0294	5° 45'	0.100
0.0588	11° 20'	0.200
0.0882	17° 28'	0.300
$T_w/T = 0.1$, $\rho/\rho_w = 0.1$, $\gamma = 1.4$.		
0.0077	5° 45'	0.100
0.0154	11° 20'	0.200
0.0231	17° 28'	0.300
$T_w/T = 0.01$, $\rho/\rho_w = 0.01$, $\gamma = 1.4$.		
0.00083	5° 45'	0.100
0.00166	11° 20'	0.200
0.00249	17° 28'	0.300
$T_w/T = 0$, $\rho/\rho_w = 0$, $\gamma = 1.4$, result is: $M_w = 0$ for all θ_t.		

(Effect of γ.)
$T_w/T = 1.0$, $\rho/\rho_w = 1.0$.

γ	M_w	θ_t	M_w	θ_t
1.2	0.047	5° 45'	0.142	17° 28'
1.4	0.045	5° 45'	0.130	17° 28'
2.0	0.040	5° 45'	0.120	17° 28'

This flow characteristic is in qualitative agreement with that revealed by the analysis of the porous-nozzle flow on the water table. Thus, one can conclude that incompressible flow studies on the water table can be used to investigate (qualitatively) the effects of massive injection on the dynamics of compressible flow in nozzles.

Before discussing the flow analogy further, we can complete this development by applying these results to a hydrogen-propelled gas-core nuclear rocket. The inlet pressure to the nozzle will be taken as 1000 atm (Kascak, (9); Ragsdale and Willis (1)); the gas inlet temperature is 20,000°R (11,100°K). The mass flow rate is 10 lbm/sec (Taylor et. al. (10)). Properties of hydrogen are taken from Kubin and Presley (11).

At the throat $P/P_0 \simeq 0.5$ and $T/T_0 \simeq 0.8$ assuming isentropic flow. So we estimate that

$$T^* \simeq 16{,}000°R$$
$$p^* \simeq 500 \text{ atm}$$
$$Z \simeq 1.90 \qquad (pv = ZRT)$$
$$\rho \simeq 0.0448 \text{ lbm/ft}^3$$

Injected coolant is assumed to be hydrogen at 500 atm and 540°R. This pressure is picked so that the wall pressure approximates the main stream pressure. The temperature represents a nominal value. Under these conditions $\rho = 2.56$ lbm/ft^3. Therefore

$$T_w/T = 0.034$$
$$\rho/\rho_w = 0.0175$$

Values of γ are 1.40 at the wall and 1.50 in the main stream. Taking $\gamma = 1.5$ and using the above data, we can solve the cubic equation for $M_{w,t}$ to find the location

for M = 1. We find

θ_t	$M_{w,t}$
5° 45'	0.00136
17° 28'	0.0040

Thus, a wall (injection) Mach number of 0.00136 will move the hydrodynamic throat 5° 45' downstream from the A* position. The blowing parameter, λ, is given as $\lambda = (\rho_w v_w)/\rho V$. At the throat, for $M_{w,t} = 0.00136$, we have

$$\lambda = (1/0.0175)(0.00136) = 0.078.$$

The above calculations illustrate the manner in which the throat characteristics can be estimated for an actual nozzle with wall injection.

DISCUSSION OF HYDRAULIC ANALOGY IN POROUS NOZZLES

The basis for the hydraulic analogy, if one exists, is obtained through a comparison of the flow equations for the water-table and compressible gas flows. For our purposes, Equations (5) and (24) are sufficient.

It is of interest to first specialize these equations for the case of an impermeable nozzle ($M_W = F_W = 0$). One obtains for the water-table and gas flows, respectively,

$$\frac{dH}{dx} = \frac{2F^2}{1-F^2}\frac{H}{B}\tan\theta \tag{26}$$

$$\frac{dT}{dx} = \frac{2(\gamma-1)M^2}{(1-M^2)}\frac{T}{B}\tan\theta \tag{27}$$

Obviously, the substitutions $M = F$, $\gamma = 2$, and $T = H$ in Equation (27) produce Equation (26) exactly. On this basis we may say that an exact analogy exists when $\gamma = 2$ and the nozzle wall is non-porous. This fact has been known for decades and is called the hydraulic analogy.

For the case of injection, Equations (5) and (24) must be compared with finite M_W and F_W. While there are similarities between the two equations, there are no simple substitutions which reduce Equation (24) to Equation (5). For this reason, a direct analogy does not appear to exist between compressible nozzle flow and incompressible open channel flows with wall injection. This may be due to the fact that with injection, the flow does not follow an isentropic process except in the trivial case of injection of the same fluid as the main stream with $v_W = V$, $T_W = T$, $\rho_W = \rho$, $P_W = P$. Also, the injection must be parallel to the main stream.

For injection through a porous wall the aforementioned conditions cannot be met. For injection through a slot, however, the conditions can be approached. Nevertheless, even then one would presumably not inject fluid at the same temperature as the main stream.

In conclusion, the nozzle flow is not isentropic when there is uniform wall transpiration, and an exact analogy does not hold. However this does not mean that analogous behavior does not occur. In fact, such behavior does occur and the required equations to investigate this have already been developed. The equations show that for compressible flow, the effect of injection is to move the position of the sonic point downstream of the geometric throat. The same effects occur for the incompressible open channel flow.

Results from the experimental portion of this investigation are presented and discussed in the next section. They show that wall transpiration indeed shifts the position at which F = 1 in the downstream direction. This is in agreement with the trend already found from the one-dimensional flow equations. Because of the close correspondence between the experimental findings and the one-dimensional flow analysis, complete numerical solutions have been obtained for the water-table equations, Equations (5) and (6). These are presented and discussed in a later section.

EXPERIMENTAL RESULTS - WATER TABLE

Qualitative

Because the emphasis in the experimental work was on observations of flow phenomena, a large number of colored slides, black and white stills, and a lesser quantity of 16 mm movies were obtained for flow with injection. Reproduction cost limit the presentation of these results to black and white stills. Figures 6, 7, 8, 9, 10 present results for the effect of injection on the flow field in the nozzle. The conditions under which the figures were obtained are listed in Table II. Figure 5 shows the nozzle as positioned on the water table. Blowing rates can be individually controlled in the three sections labeled I, II, and III on the Figure.

The flow visualization technique, described in detail in (4), produces color differences between fluid streams without the use of permanent dyes. This is accomplished through pH control of the two streams and a suitable acid-base indicator (bromothymol-blue) mixed in the fluid. The injected fluid is made basic with the addition of sodium hydroxide; the main flow is an aqueous solution of acetic acid.

Figure 6 notes flow without injection. The expansion fan is evident in the divergent portion of the nozzle. The variation in water height (in the direction perpendicular to the plane) produces a pronounced distortion of the straight lines ruled at one inch intervals along the table surface. (The lines ruled across the channel are not at one inch intervals).

Figures 7a and 7b compare injection at low and high rates in section I. Since here the main stream velocity is low the injected fluid can penetrate well into the main flow. Thus injection of 1.85% (per wall) of the inlet mass flow (Figure 7a) produces a thick, well defined layer in the converging portion of the nozzle.

Figures 8a and 8b compare injection at low and high rates in the second section of the nozzle. With 1.45% injection per wall only a very thin protective layer is

TABLE II FLOW CONDITIONS FOR FIGURES 6 TO 10

Figure[+]	Injection Conditions: Section I $\dot{m}_I/\dot{m}_{inlet}$*	Section II $\dot{m}_{II}/\dot{m}_{inlet}$	Section III $\dot{m}_{III}/\dot{m}_{inlet}$
6	0	0	0
7a	3.9%	0	0
7b	8.2%	0	0
8a	0	2.9%	0
8b	0	7.6%	0
9a	3.1%	5.7%	0
9b	3.1%	3.1%	3.1%
10a	1.5%	1.5%	1.5%
10b	6.6%	6.6%	3.3%

[+]Plus-x Film, ASA 125, top and bottom lighting, 1/125 at f8 exposure.

*Injection from both sides so 8.2% represents 4.1% from each side.

provided at the throat. With substantial injection of 3.8% of the inlet mass flow, Figure 8b, a well defined thick layer is provided. In this region the main stream velocity is about 1.6 ft/sec at the throat, and the injected flow does not penetrate very far into the main flow.

Figures 9a and 9b contrast blowing in the first two sections with blowing in all three sections. Blowing in the third section produces pronounced enhancement of the surface waves in the divergent portion of the channel; compare Figure 6 with Figure 9b.

Figures 9b, 10a, and 10b are for blowing in all three sections at total injection mass flows of 9.3%, 4.5%, and 16.5%, respectively. The injected layer maintains its integrity rather well considering the effects of vertical accelerations disturbing the flow in the transonic region of the nozzle.

Even massive injection does not adversely affect the main stream flow. The injected layer remains intact, and while mixing at the interface occurs, the main stream does not penetrate to the wall in any of the cases with injection in all three sections. It will be seen that these pictures correspond closely to those obtained with the gas flow test section.

It seems appropriate at this point to comment on the magnitude of the mass injection. The usual parameter to describe injection is

$$\lambda = \rho_w v_w / \rho V$$

This is suitable for external flow but for internal flow a better parameter might be

$$\lambda_{int} = \rho_w v_w A_w / (\rho V A)_\infty$$

If ρ_w and v_w are functions of position, then an integrated value is required along the wall. The reason that λ is not fully descriptive for internal flow is that a small

value can still lead to large ratios of $\dot{m}_{inj}/\dot{m}$ if the injection occurs over a big area. Thus a more appropriate quantity must include the area for wall injection.

Since water table results are for incompressible flow, $\rho_w = \rho$ and λ reduces to

$$\lambda = v_w/V = F_w/F$$

Typically at the throat $V_t \simeq 1.6$ ft/sec and a typical value for the wall velocity is $v_w = 0.03$ ft/sec. Thus $\lambda = 0.03/1.6 \simeq 0.02$.

Quantitative

Figure 11 shows the no-injection Froude number as a function of position in the nozzle. The two-dimensionality of the flow field is evident. Froude number distributions are obtained by measuring the local water depth to obtain $\sqrt{gH}$. The water depth is determined by measuring with a pointed depth micrometer the distance to the water surface and the distance to the table surface. The difference is the local water height. The Froude number is then determined from Equation (28).

Also shown in Figure 11 is the corrected Froude number (corrected to a Mach number corresponding to $\gamma = 1.4$). The correction, previously discussed, is particularly significant at high values of F.

Figure 12 shows Froude distributions with and without blowing. The solid curves correspond to the case of no injection, and the dashed curves show the effect of wall blowing. The blowing conditions are similar to those in Figure 10b and the relative rates of injection through the three sections are as indicated. It is seen that the effect of injection is to move the critical "line" F = 1 downstream.

INCOMPRESSIBLE SOLUTION

COMPUTATIONAL PROCEDURE AND RESULTS

The governing equations for incompressible flow with injection were derived previously. Equations (5) and (6) are coupled nonlinear, first order, differential equations which can be solved to yield numerical predictions for Froude number and the liquid-height spatial distributions.

Runge-Kutta's fourth-order integration scheme was used to integrate these nonlinear equations. The error introduced is known to be of order $(\Delta x)^5$. The Δx increment was varied from 0.0001 to 0.01 with the minimum value being at the throat region where the slope changes are the largest. The curves $F(x)$ and $H(x)$ are very smooth and hence the error introduced is not significant.

To insure the continuity of dH/dx and dF/dx at the hydrodynamic throat, integration commenced at that point. By picking the value of θ_t between 0° and 15°, the value of $F_{w,t}$ was computed from Equation (10) and then the injection velocity from $v_w = F_{w,t}\sqrt{gH_t}$. The value of liquid height at the throat was chosen to correspond closely to the experimental heights of order 1 to 1.5 inches. However, it has no bearing on the dimensionless height ratio (local height to stagnation height) or the local Froude number. For the given θ_t, the height and Froude number slopes were determined from Equations (12) and (6), respectively, and the values of H and F calculated a Δx increment away. This was done for several minimum step sizes, sufficiently away from the region of instability of Equation (5). Afterwards, Equations (5) and (6) were exclusively used in the Runge-Kutta scheme of integration, first upstream of the hydrodynamic throat and then downstream of it. The injection velocity (and thus F_w) could be varied at each step (or set equal to zero, if so desired, as was done for the region upstream of the straight 45° convergence portion of the nozzle). In this manner, comparisons could be made with experimental data.

The calculations were not carried to the extreme upstream region. Rather the stagnation height was determined from the expression

$$H_o = H(x)[1 + 0.5\ F^2(x)] \qquad (28)$$

which is a statement of the conservation of energy along the streamline. The numerical results are presented graphically. The nozzle of interest, already noted in Figure 5, is divided into three sections in which blowing rates can be individually controlled. These are labeled I, II, III in the Figures.

Mass injection has a significant effect on the Froude number, especially in the supercritical region as may be seen in Figure 13. The parameters are θ_t and $\dot{m}_{inj}/\dot{m}_{inlet}$. For $\dot{m}_{inj}/\dot{m}_{inlet}$, a value of 0.13 corresponds to total injection equal to 13% of the inlet mass flow. Since the injected mass x-momentum is only a small fraction of the main stream momentum (in the convergent nozzle section the injected x-component is negative), the mainstream mass must impart some of its kinetic energy to accelerate the injected mass. This manifests itself in a lower Froude number as compared to flow without injection. Since the kinetic energy is proportional to the square of the velocity, the energy expended by the main stream mass to accelerate the injected mass in the supercritical region is accordingly much greater than in the subcritical region. Hence divergence of the Froude lines from the no-injection case is more pronounced when injection takes place in the supercritical region. Note that the effect of injection is to move the position at which F = 1 downstream of the geometric throat.

Figure 13 also depicts the H/H_o curves for two injection ratios, again defined as a percentage of the mainstream inlet flow rate. The increase in height ratio is confined mainly to the supercritical region. The effect of injection is to decrease the mainstream velocity at a given x-location. This is accompanied by a local increase in the liquid height since continuity must be preserved. Thus the effect on the Froude number is compounded, because F is proportional to V and inversely proportional to $\sqrt{H}$. This is clearly exhibited in the figure, the influence on H/H_o being much smaller than on F.

Figure 14 indicates results for F for the case of injection in sections I and II of the porous nozzle. For a total injection equal to 31% of the inlet flow, the

position at which F = 1 is shifted downstream about 0.25 inches. This corresponds to the "sonic" line occurring at $\theta = 5°$, as opposed to $\theta = 0°$.

Figure 15 indicates the blown-layer thickness, δ, as a function of position for various flow conditions. These results were calculated from Equation (13) and assume no mixing with the free stream flow. They therefore represent minimum distances for which the effects of blowing are felt.

The conditions for which these results were obtained correspond to blowing in sections I, II, and III, with equal v_w in all three sections. In particular, for a total injection of 13% of the inlet mass flow, the injection velocity was 0.34 inches/sec. For an injection of 20%, $v_w = 0.51$ in/sec and for 39%, $v_w = 0.60$ in/sec. Since the water height is markedly dropping through the nozzle, the injected mass flow is not equal in each section. The shape of the $\delta(x)$ curves is as noted because of this change in water height. In a gas nozzle, if injection occurred at the local pressure and with the same wall velocity at all locations in the nozzle, a similar shape should result. This is because the fluid density decreases in the flow direction.

Figure 12 has already presented experimental results for the Froude number distribution with and without blowing. The data on this figure are for a total injection rate of 21.1% of the inlet flow, with an injection equal to 16.6% of the inlet flow in the first two sections. The F = 1 position along the centerline is shifted about 0.2 inches downstream. The results of Figure 14 indicate a similar downstream shift in the "sonic" position. Thus the experiments and analysis show satisfactory agreement for the incompressible case with injection.

EXPERIMENTAL RESULTS - GAS TUNNEL

Late in the experimental program it was decided to utilize the Aerospace and Mechanical Engineering Department's small supersonic facility for a flow visualization study of gas injection into a main stream air flow. Schlieren pictures were obtained with a spark light source for CO_2 and Freon-12 injected through the porous walls of a nozzle geometrically similar to that used on the water table. Pictures for injection of air were obtained using a continuous light source.

The wind tunnel is an in-draft type facility, and about 45 seconds of run time can be obtained. No quantitative results were attempted for this report. However a subsequent report on a nozzle with discrete slot injection includes some transient pressure results. In this respect the water table offers a real advantage since detailed fluid studies can be made over several hours of operation at the same flow conditions.

Figure 16 shows the porous-walled nozzle used in the supersonic tunnel. Blowing rates could be independently controlled in each of the three sections. The section dividers are shown cross-hatched.

Table III summarizes the flow conditions for Figures 17, 18, 19, 20, and 21. Figure 17 shows the flow with no injection. Figure 18 is a composite picture corresponding to injection of air into air. With air as the injectant, only small density gradients occur. Thus the injected layer is visible only in the supersonic portion of the nozzle. The upper half of the figure shows details of the flow with no wall injection. The lower half corresponds to wall blowing with a total injection of 16.5% of the inlet mass flow, distributed as 3.3% for each side of section I, 3.3% for each side of section II and, 1.65% for each side of section III. The oblique wave pattern in the divergent portion of the nozzle is qualitatively the same as that found on the water table (Figure 7).

Figures 19a and b show Freon-12 injection through all three sections. Figure 19a shows the effect of a low injection rate and 19b a high rate. Figures 20a, b, and c are for CO_2 injection. Figure 20a has an injection of

TABLE III FLOW CONDITIONS FOR FIGURES 17 TO 21

Figure	Injection Conditions: Section I* $\dot{m}_I/\dot{m}_{inlet}$+	Section II $\dot{m}_{II}/\dot{m}_{inlet}$	Section III $\dot{m}_{III}/\dot{m}_{inlet}$
17	0%	0%	0%
18 (air)	6.6	6.6	3.3
19a (freon)	3	3	3
19b	12	12	12
20a (CO_2)	3	3	3
20b	6	6	6
20c	12.5	0	0
21a (freon)	12	0	0
21b	0	12	0
21c	12	12	0

* injection from both sides so 6% is 3% from each side.

+ calculated from one-dimensional flow theory.

1.5% of the inlet mass flow (calculated from one-dimensional flow theory without blowing) in each section and on each side. Thus the overall injection rate is 9% of the inlet mass flow. Figure 20b shows CO_2 injection at 3% of the inlet mass flow in each section and both sides (18% total injection). Figure 20c shows an injection from section I only. The injection rate is 12.5% (total from both sides) of the inlet flow. Figures 21a, b, and c are for Freon-12 injection from sections I, II, and I and II, respectively.

For all of these cases it can be seen that injection does not disturb the mainstream flow pattern markedly from that found with no injection.

It is possible to calculate an approximate value for the blowing parameter, λ, from the data. The mass flow to each section was metered. Knowing the injection area, the product $(\rho v)_{inj}$ can thus be calculated. The product $(\rho V)_\infty$ can be calculated from one dimensional theory without injection. These have been obtained using the area ratios at the midpoint of the injection sections. The values of $\lambda = (\rho v)_{inj}/(\rho V)_\infty$ thus obtained are given in Table IV.

For section I, $(\rho V)_\infty$ is quite low so λ is very large. In turn, this means that a thick injected layer can be expected. This is verified in Figure 20c. This layer is carried smoothly through the throat, and with some additional, but lesser, injection in the throat region, should provide good thermal protection for the wall. Not surprisingly, λ is low in the throat region, and injection there provides only a very thin layer; see Figure 21b.

The qualitative agreement between these figures for compressible flow and the previous figures for flow on the water table is good. On the water table, injection in the subsonic region also produced a thick layer, but transonic injection results in only a thin layer.

It is important to note that the thickness of the injected layer is not a linear function of the mass injected. The low injection rates produce almost as thick a layer as do the very large injection rates (i.e. Figure 20a with 9% compared to Figure 20b with 18%). This is probably due to the increase in the main stream pressure (at a given position) as the amount of injection increases. Thus doubling the injected mass flow also increases the

TABLE IV BLOWING PARAMETER, λ, FOR SEVERAL MASS INJECTION RATIOS

$$\lambda = (\rho v)_{inj}/(\rho V)_{\infty}$$

Section	$\frac{\dot{m}_{inj}}{\dot{m}_{inlet}}$ 1%	3%	6%	10%
I	0.095	0.28	0.56	0.95
II	0.0094	0.028	0.056	0.094
III	0.0115	0.0345	0.069	0.115

density (and thus the momentum for a given velocity) of the mainstream fluid. As a result, λ is not doubled. This parameter is believed to be more important in correlating penetration depth than the mass injection ratio.

DISCUSSION OF RESULTS

The results of the one-dimensional analysis for both incompressible and compressible flow have indicated that the position of the hydrodynamic throat is moved downstream of the geometric throat because of injection. The more the injection, the greater the change in the position of the hydrodynamic throat. Without injection it is well known that the two-dimensionality of compressible flow in a nozzle causes the sonic position to be downstream of the minimum flow area. The effect of injection is to exaggerate this effect.

While no direct analogy could be established between compressible and incompressible flow, both with injection, analogous behavior was noted. For the case of no injection the hydraulic analogy indicates that Froude number results are equivalent to Mach number results for a gas with $\gamma = 2$. With injection such a simple relationship could not be established, but the results, both analytical and experimental, clearly indicate that water table results can be used to predict qualitatively what changes will take place in a gas nozzle with injection.

The incompressible experimental results for the porous nozzle show that even with massive injection (where $\dot{m}_{inj}$ is of the order of 20% of the inlet mass flow) the main stream flow is not seriously disturbed. A one-dimensional analysis could probably be used to estimate the flow field if the area used in the calculation were the actual geometric area less the area required for the injected layer.

The compressible experimental results, using a Schlieren system to visualize the flow field, also indicate that massive blowing does not cause unusual phenomena to occur in the flow. The blown layer stays close to the wall and does not, for example, mix rapidly with the core flow. A potential problem was, however, noted which affects the thermal protection at the nozzle throat. It is difficult with a porous nozzle to obtain a thick blown layer at the throat region. The extreme axial acceleration at this point causes injected fluid to be moved downstream before penetrating very far into the mainstream. To obtain a thick layer at the throat, it is

necessary to have large injection upstream of the throat so that the blown layer can be swept through the throat intact and adjacent to the nozzle wall. Alternatively, one might obtain a thick wall layer at the throat by injecting fluid through a single (or multiple) slot upstream of the throat.

CONCLUSIONS

1. The Froude number at a given location in the supercritical region of the nozzle decreases considerably with increased rate of injection. In the subcritical region, the decrease is much less pronounced.

2. Wall injection moves the hydrodynamic throat downstream from the physical throat.

3. The calculated injected boundary layer thickness, based on a uniform plug-flow model, is approximately half as thick as the visualized layer. This is probably because in the calculations, an assumption was made that no mixing occurs between the injected and main stream fluids.

4. For fixed stagnation conditions, the total flow rate through the nozzle is not altered significantly by injection. The mainstream inlet flow rate is diminished by the amount of the injection upstream of the throat.

5. Experimental results for both incompressible and compressible flow indicate that for blowing rates as large as 20% of the inlet mass flow rate, no serious disturbances occur in the flow field. The Froude and Mach number distributions are modified from the no-injection case, but the flow field remains smooth through the transcritical region of the nozzle.

6. Schlieren pictures for the compressible nozzle flow indicate that it is difficult to obtain a thick blown layer at the nozzle throat unless significant injection takes place in the upstream, subsonic region.

NOMENCLATURE

A = flow area
B = width of flow
c_p = specific heat at constant pressure
F = Froude number, $V/\sqrt{gH}$
H = height of fluid
h = enthalpy
M = Mach number
$\dot{m}$ = mass flow
P = static pressure
R = gas constant
T = temperature
V = flow velocity
v_w = injection velocity
γ = ratio of specific heats of gas
δ = blown layer thickness
ρ = density
θ = angle
λ = blowing parameter

Subscripts

inj = injected
inlet = at inlet to nozzle (before injection)
o = stagnation conditions
t = nozzle throat
w = at the wall
∞ = at main stream conditions

REFERENCES

1. Ragsdale, R. G. and Willis, E. A., Jr., Gas Core Rocket Reactors, A New Look, NASA TM X-67823, June 1971.

2. Adams, D. M., Application of the Hydraulic Analogy to Axisymmetric Nonideal Compressible Gas Systems, J. Spacecraft, 4, p. 359-363, 1967.

3. Fike, R. L., Kinney, R. B., and Perkins, H. C., The Design of a Research Water Table, NASA CR 121255, August 1973.

4. Cielak, Z., Kinney, R. B., and Perkins, H. C., Flow Visualization Experiments in a Porous Nozzle, NASA CR 121256, August 1973.

5. Preiswerk, E., Application of Methods of Gas Dynamics to Water Flow With Free Surfaces, Part I, Flow With No Energy Dissipation, NACA TM 934, 1940, (translated from German).

6. Preiswerk, E., Application of Methods of Gas Dynamics to Water Flow With Free Surfaces, Part II, Flow With Momentum Discontinuities, NACA TM 935, 1940, (translated from German).

7. Loh, W. H. T., Theory of the Hydraulic Analogy for Steady and Unsteady Gas Dynamics, from Modern Developments in Gas Dynamics, Plenum Press, New York, 1969.

8. Cuffel, R. F., Back, L. H., and Massier, P. F., Transonic Flow Field in a Supersonic Nozzle With Small Throat Radius of Curvature, AIAA J., 7, p. 1364-1366, 1969.

9. Kascak, A. F., Nozzle and Cavity Wall Cooling Limitations on Specific Impulse of a Gas-Core Nuclear Rocket, NASA TM X-67923, November 1971.

10. Taylor, M. F., Whitmarsh, C. L., Jr., Sirocky, P. J., Jr., and Iwanczyk, L. C., The Open-Cycle Gas-Core Nuclear Rocket Engine - Some Engineering Considerations, NASA TM X-67932, 1971.

11. Kubin, R. F., and Presley, L. L., Thermodynamic Properties and Mollier Chart for Hydrogen from 300°K to 20,000°K, NASA SP-3002, 1964.

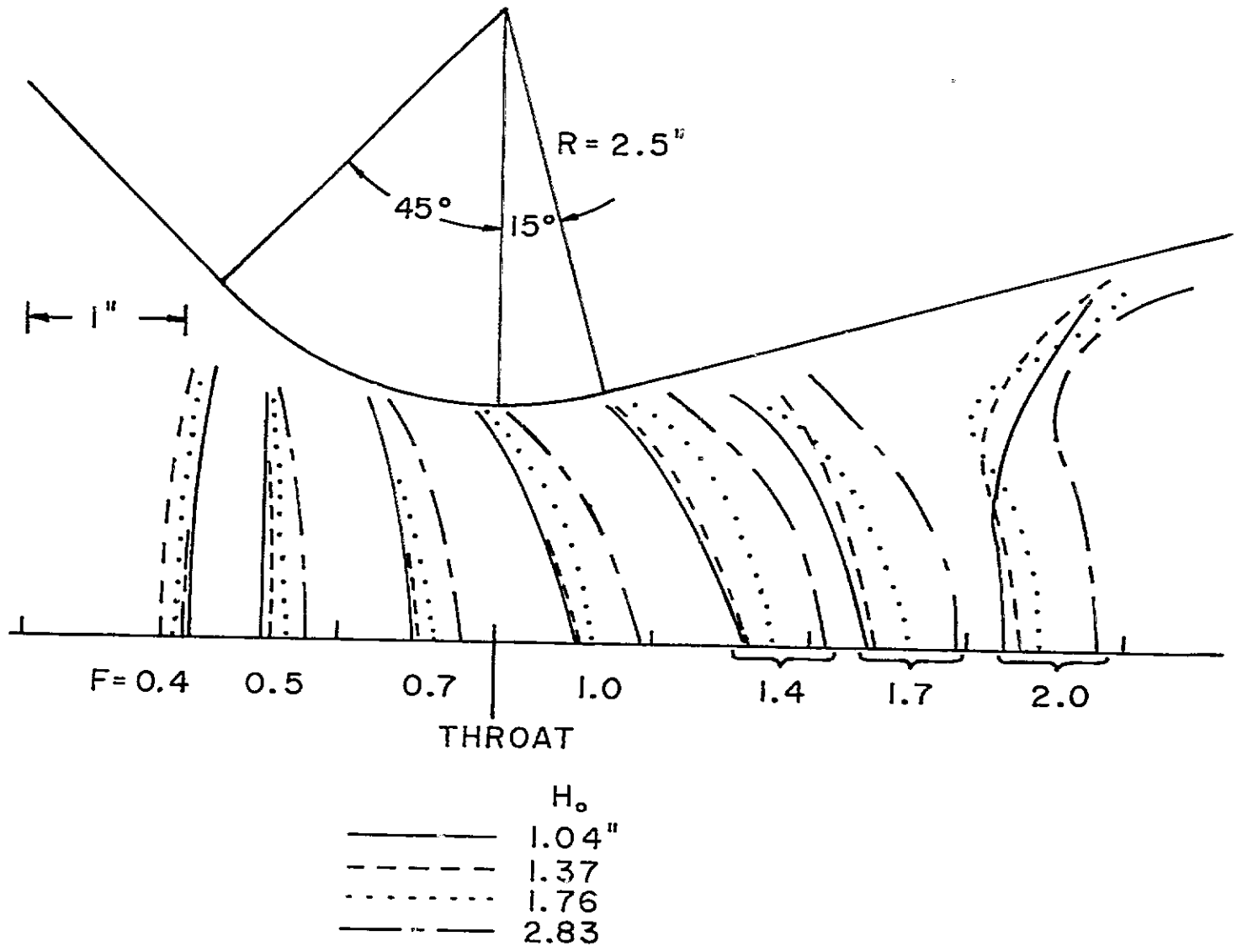

FIGURE 1 FROUDE NUMBER AS A FUNCTION OF POSITION AND STAGNATION HEIGHT - NO INJECTION.

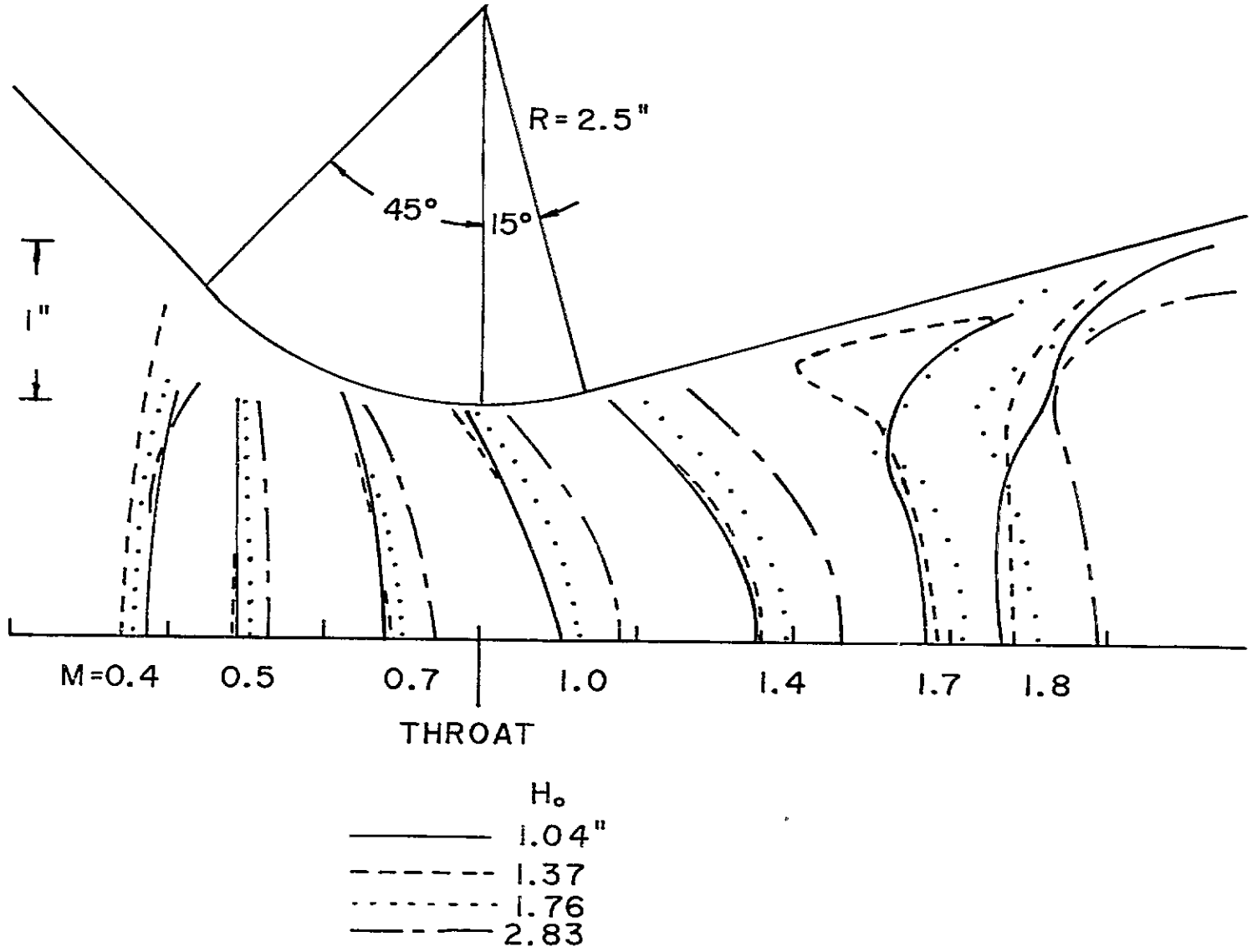

FIGURE 2 MACH NUMBER AS A FUNCTION OF POSITION AND STAGNATION HEIGHT - NO INJECTION.

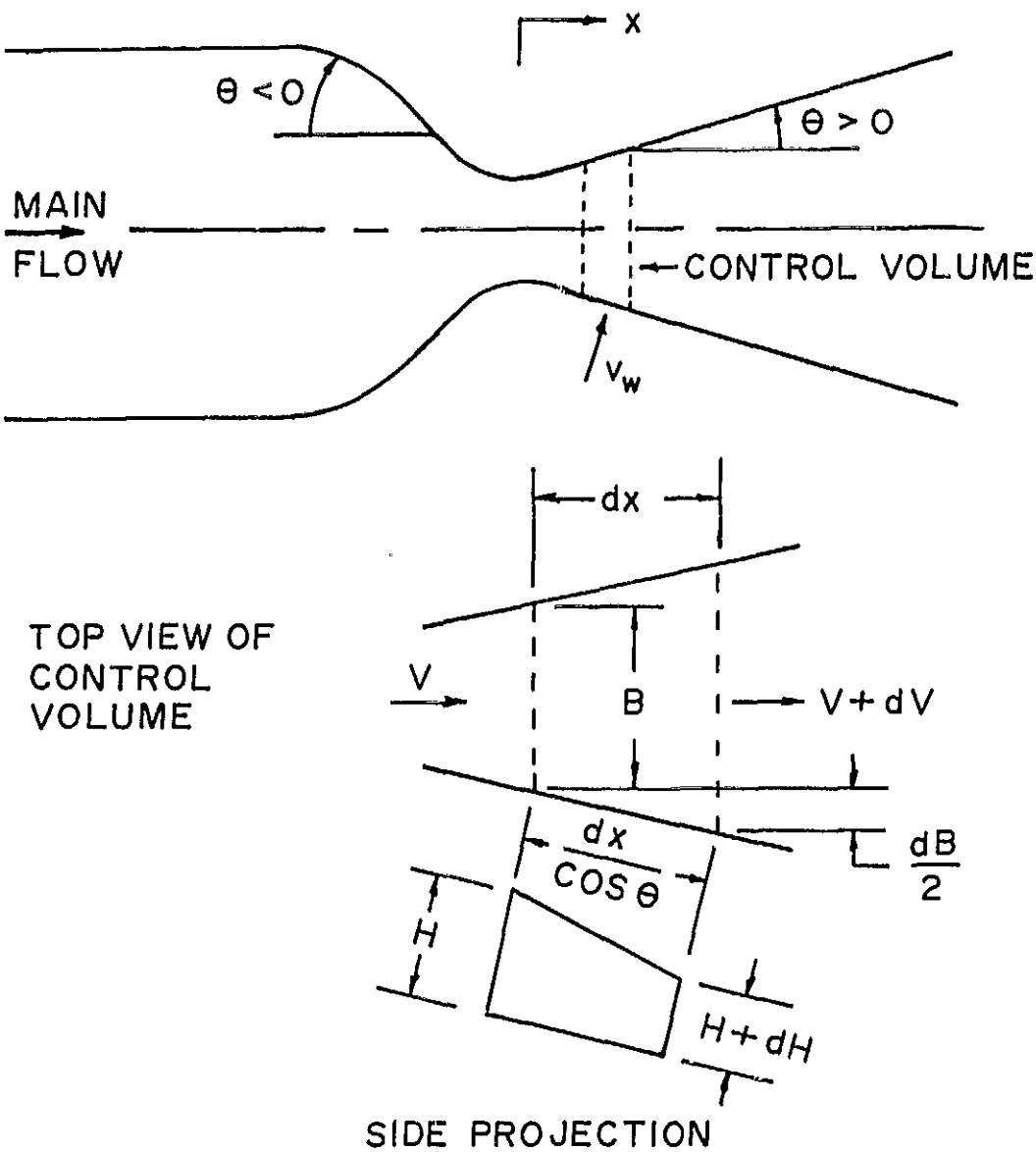

FIGURE 3 SCHEMATIC OF NOZZLE SHOWING SYMBOLS AND CONTROL VOLUME.

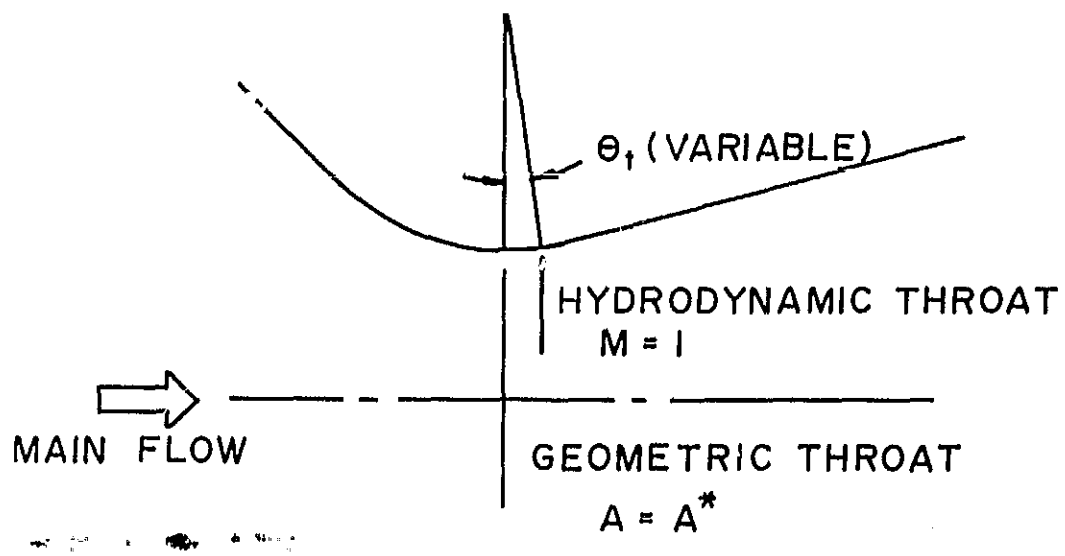

FIGURE 4 EFFECT OF INJECTION ON POSITION OF HYDRODYNAMIC THROAT.

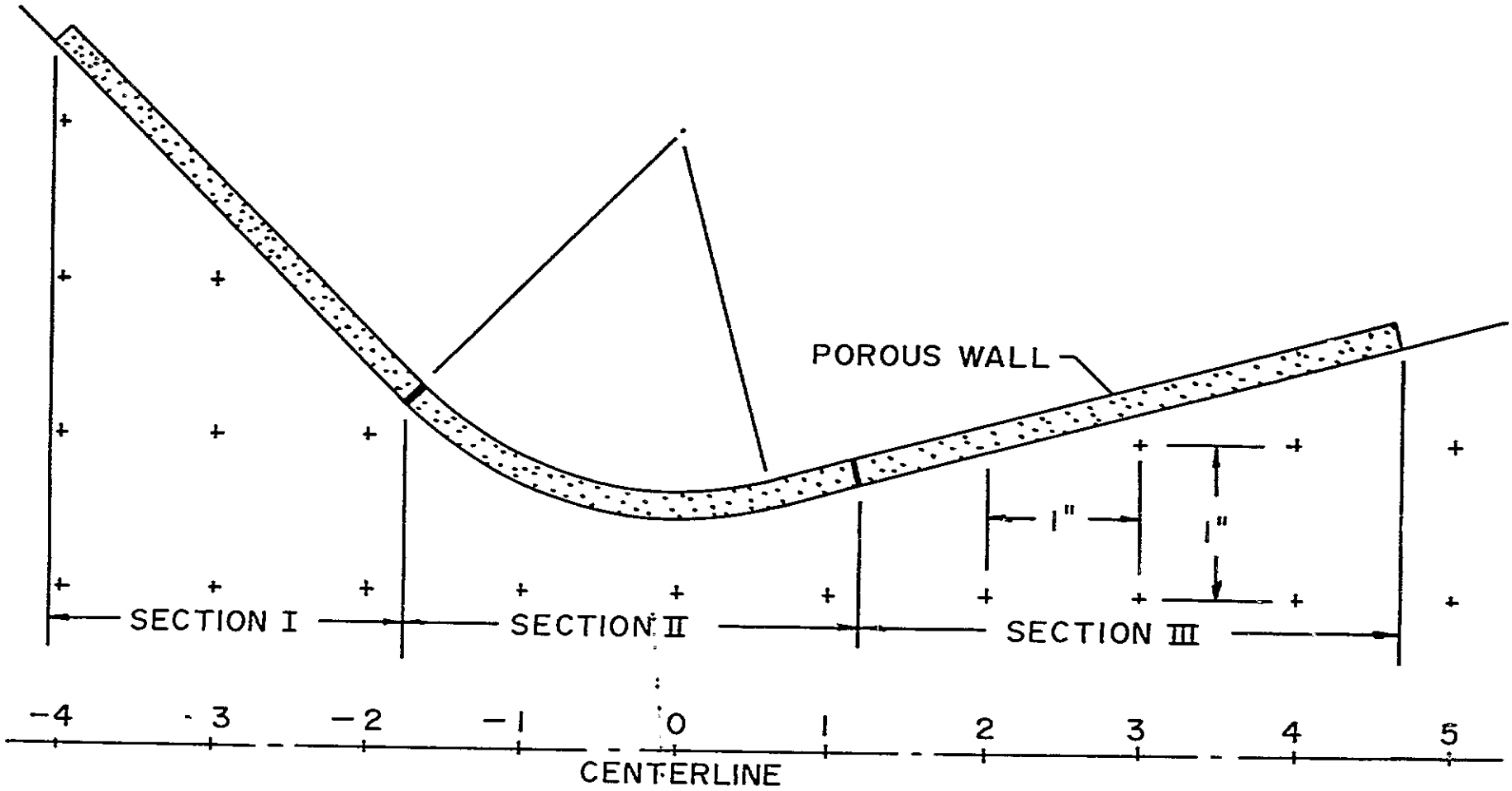

FIGURE 5 FULL SCALE DRAWING OF NOZZLE SHOWING POROUS WALL SEGMENTS.

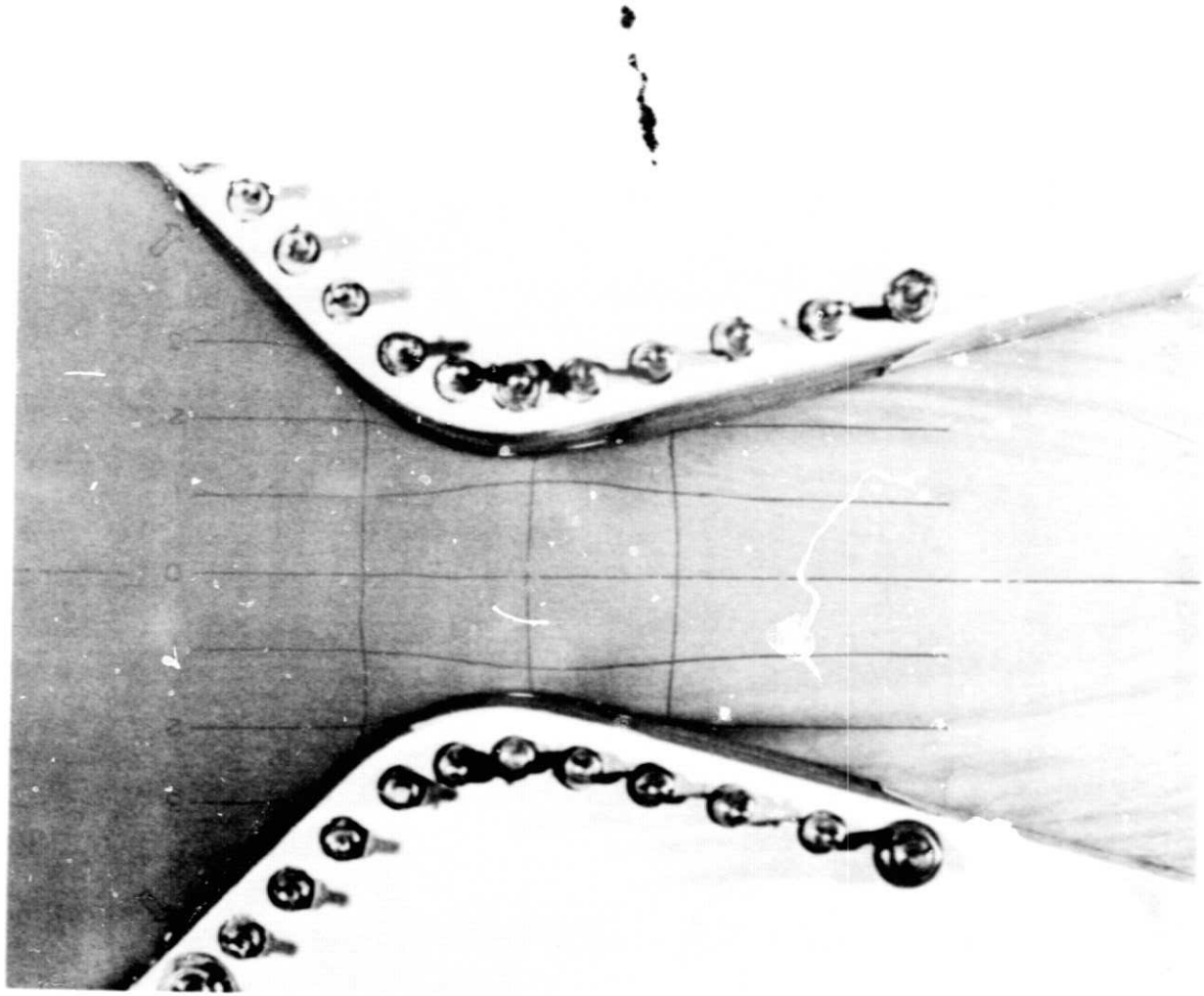

FIGURE 6 FLOW ON WATER TABLE WITHOUT INJECTION.

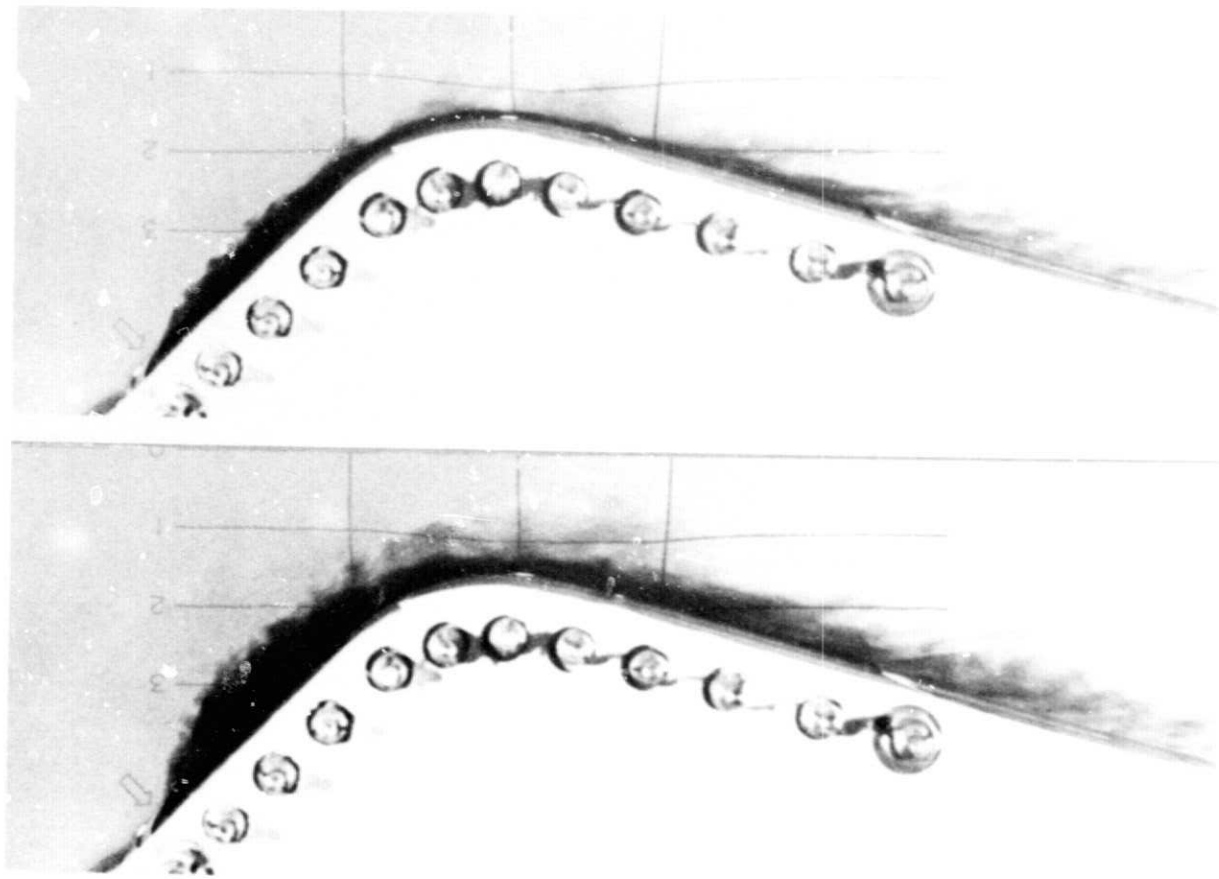

FIGURE 7a FLOW WITH LOW INJECTION RATE IN SECTION I.

7b FLOW WITH HIGH INJECTION RATE IN SECTION I.

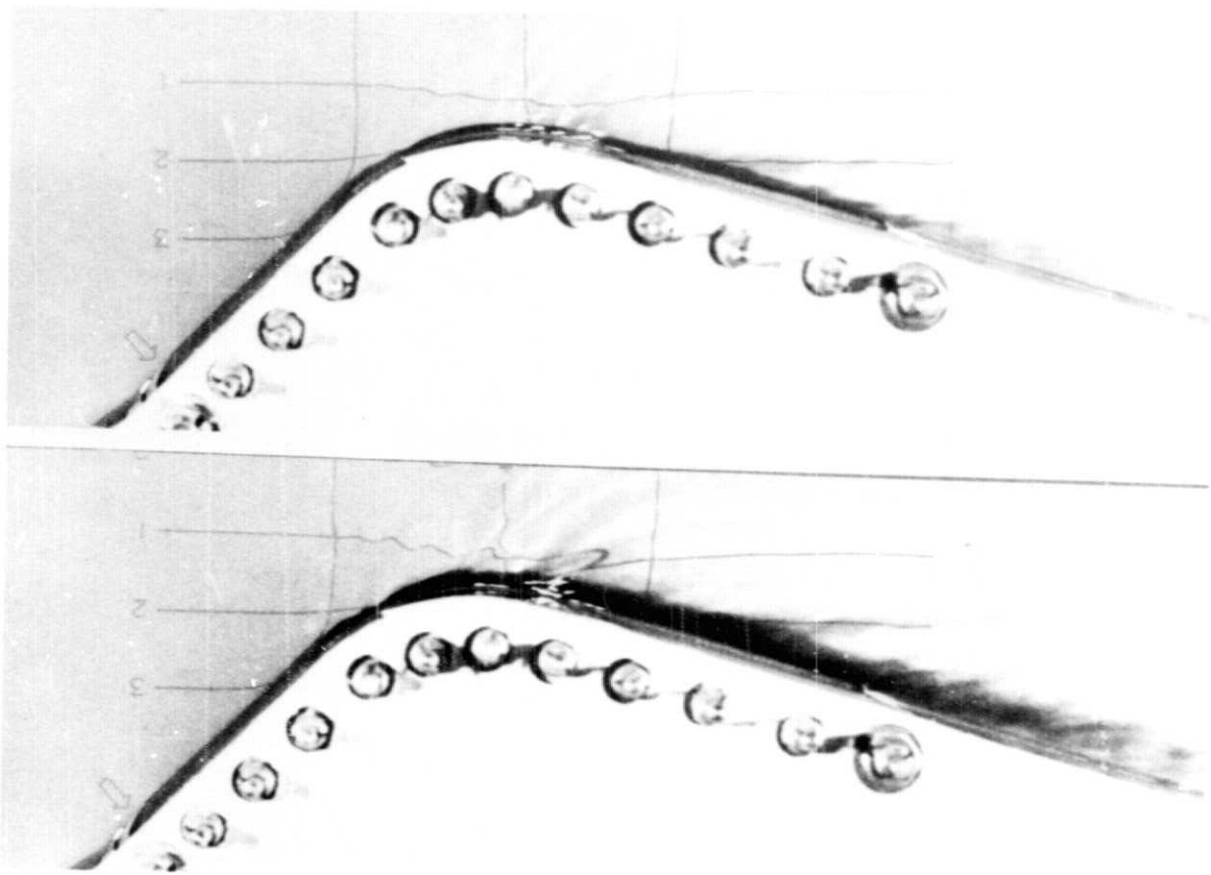

FIGURE 8a FLOW WITH LOW INJECTION RATE IN SECTION II.

8b FLOW WITH HIGH INJECTION RATE IN SECTION II.

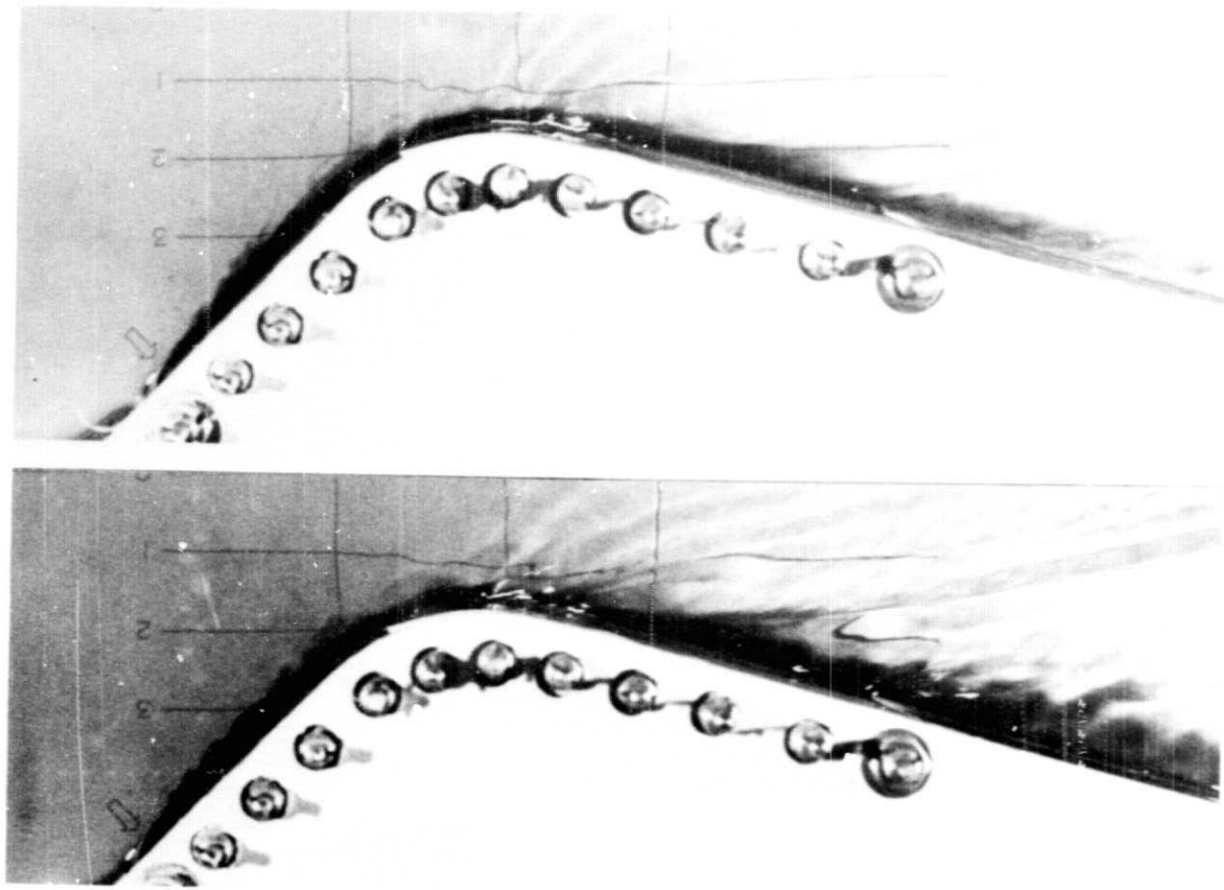

FIGURE 9a FLOW WITH INJECTION IN SECTIONS I AND II.

9b FLOW WITH INJECTION IN ALL THREE SECTIONS.

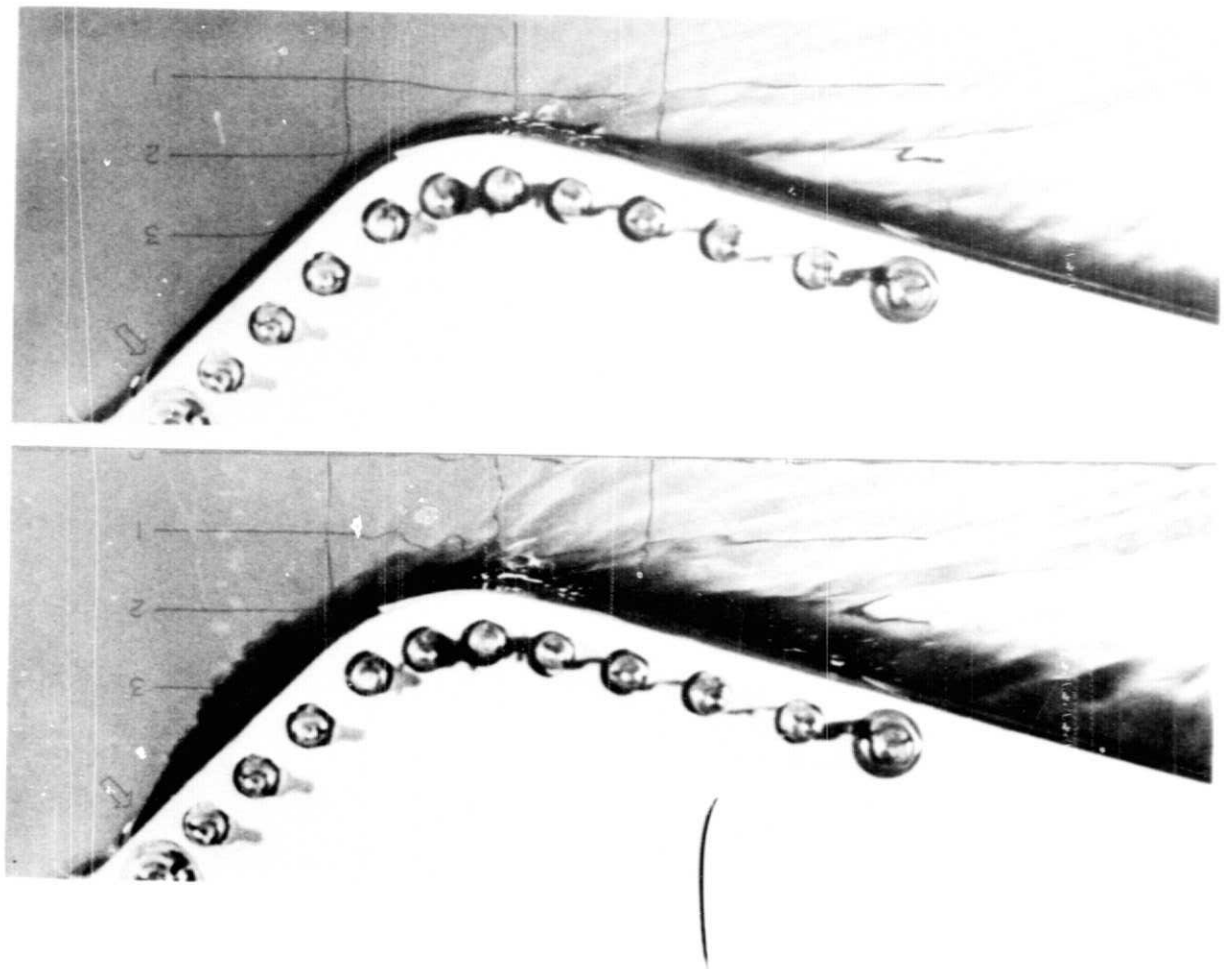

FIGURE 10a FLOW WITH LOW INJECTION RATES IN ALL THREE SECTIONS.

10b FLOW WITH HIGH INJECTION RATES IN ALL THREE SECTIONS.

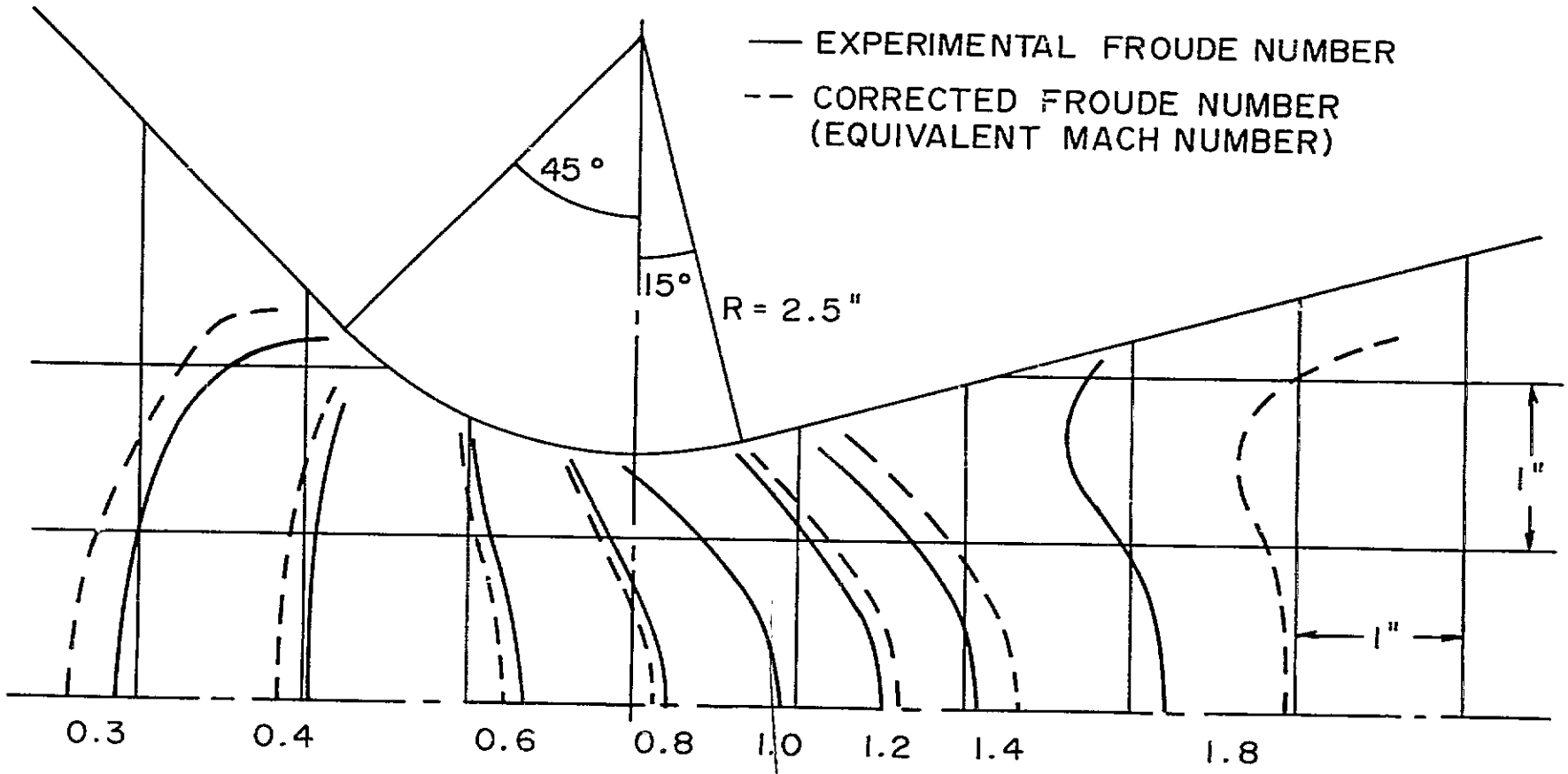

FIGURE 11 CONTOURS OF CONSTANT FROUDE NUMBER WITHOUT INJECTION (H_o = 2.83 inches).

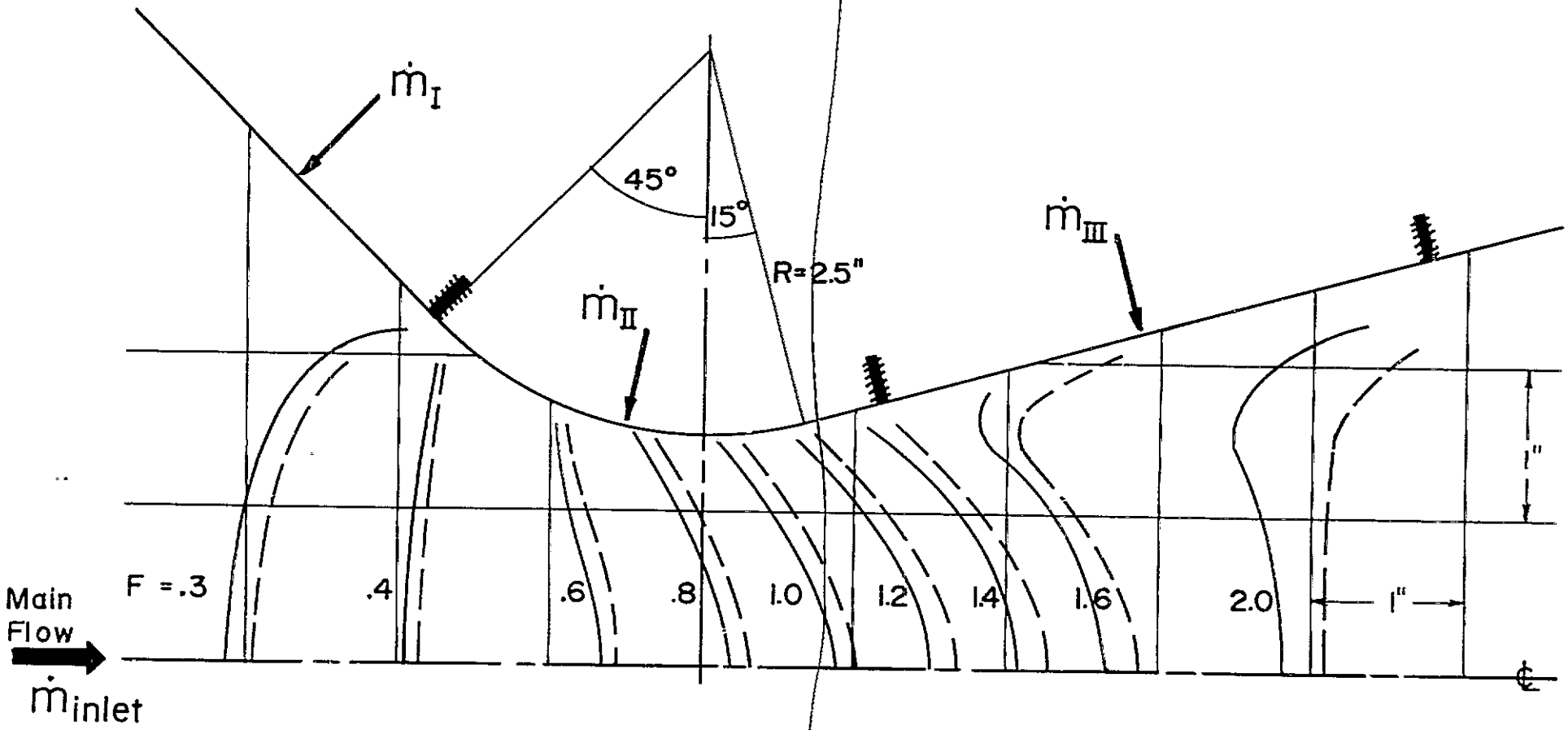

FIGURE 12 EFFECT OF INJECTION ON FROUDE NUMBER DISTRIBUTIONS.

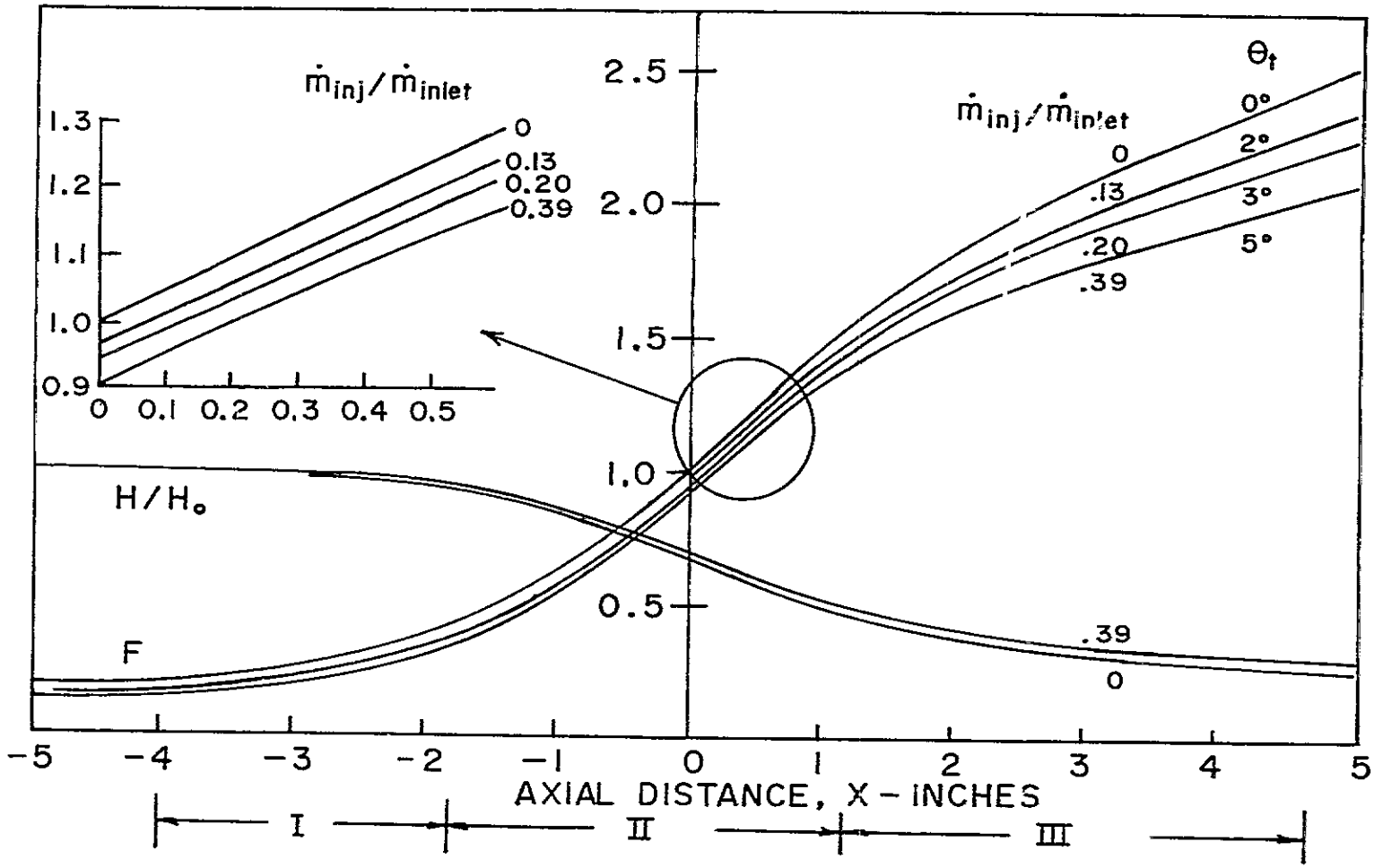

FIGURE 13 PREDICTED FROUDE NUMBER AND HEIGHT DISTRIBUTIONS WITH INJECTION IN ALL THREE SECTIONS ($v_{wI} = v_{wII} = v_{wIII}$).

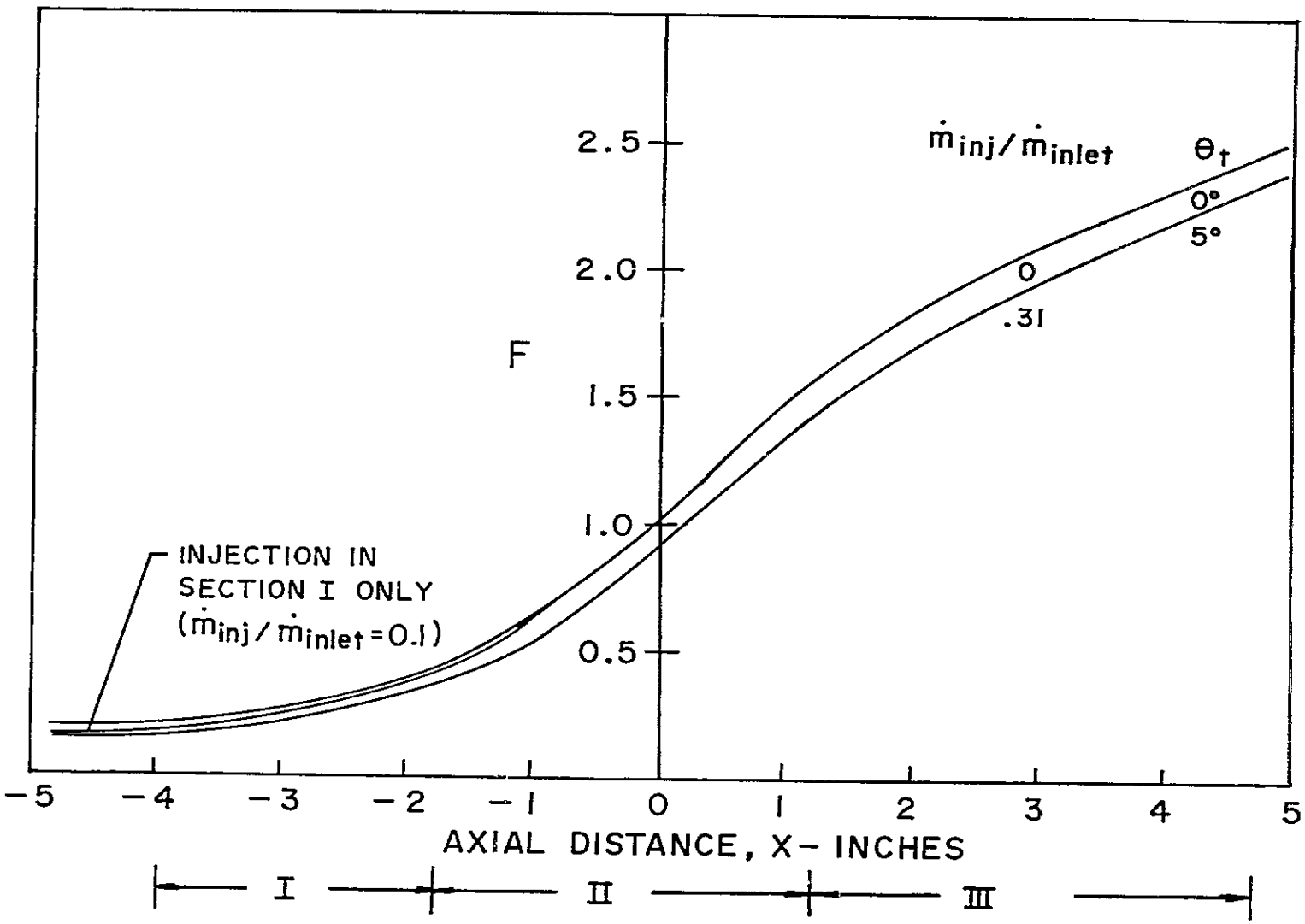

FIGURE 14 PREDICTED FROUDE NUMBER DISTRIBUTIONS WITH INJECTION IN SECTIONS I AND II ($v_{wI} = v_{wII}$).

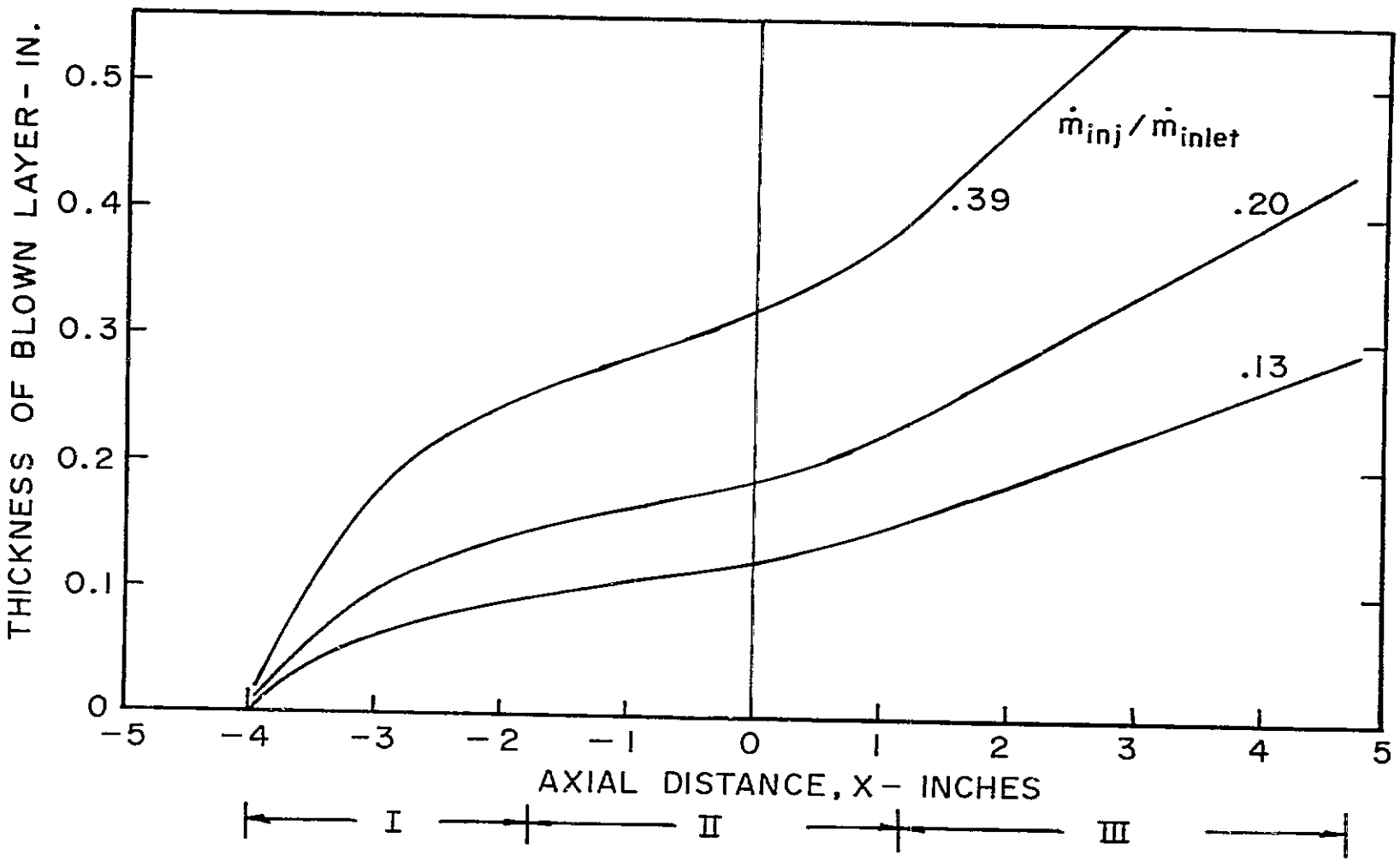

FIGURE 15 EFFECT OF INJECTION ON THICKNESS OF BLOWN LAYER ($v_{wI} = v_{wII} = v_{wIII}$).

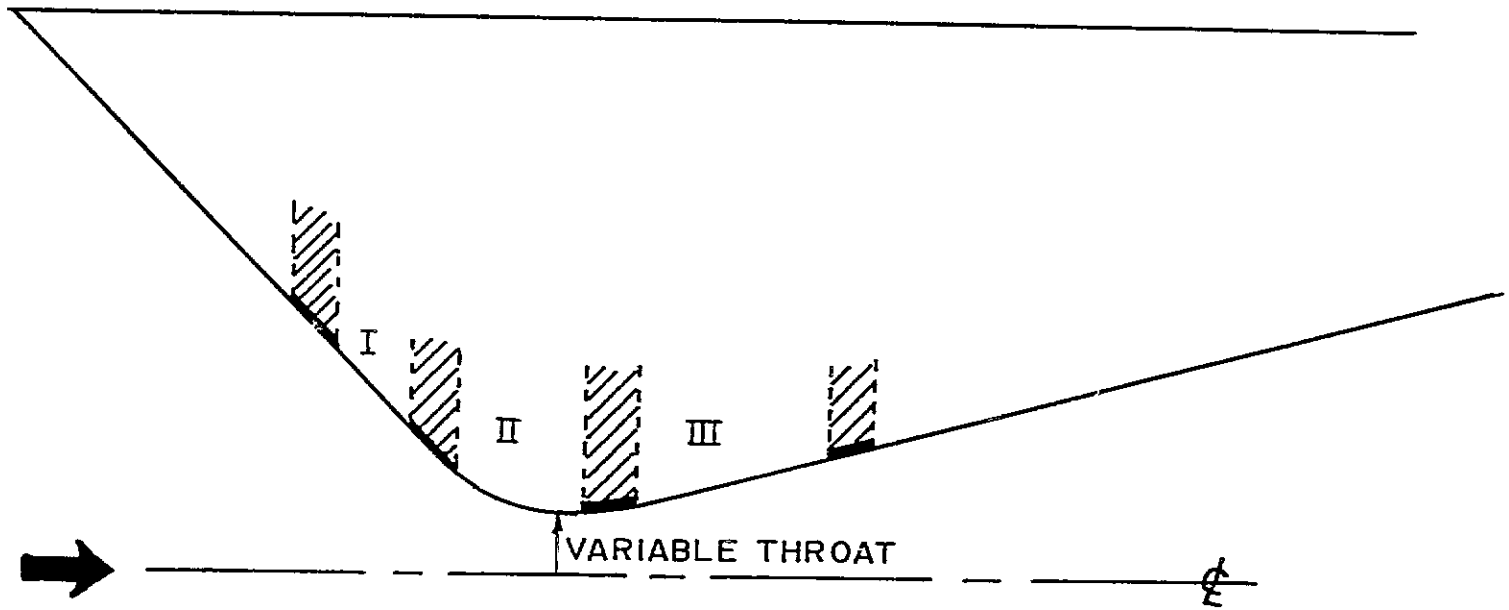

FIGURE 16 FULL SCALE DRAWING OF NOZZLE USED IN WIND TUNNEL.

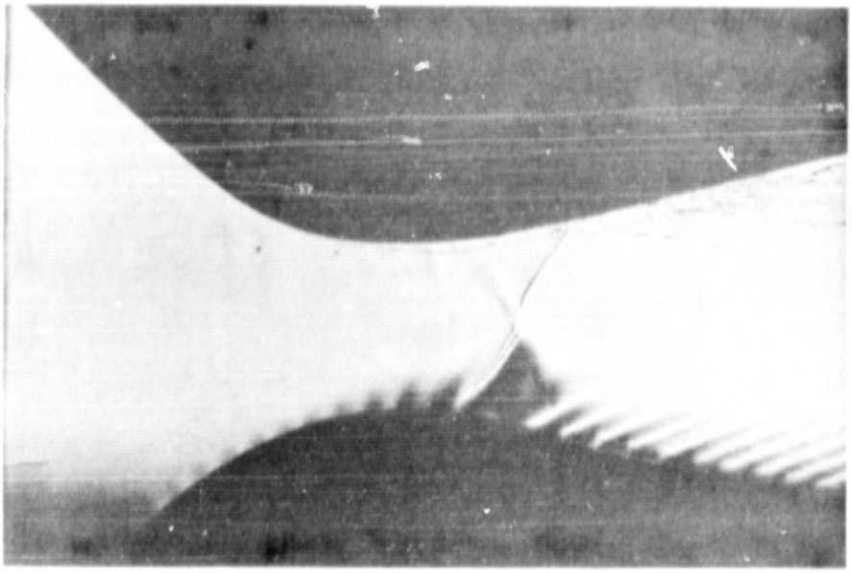

FIGURE 17 SCHLIEREN PHOTOGRAPHS OF AIR FLOW WITHOUT INJECTION.

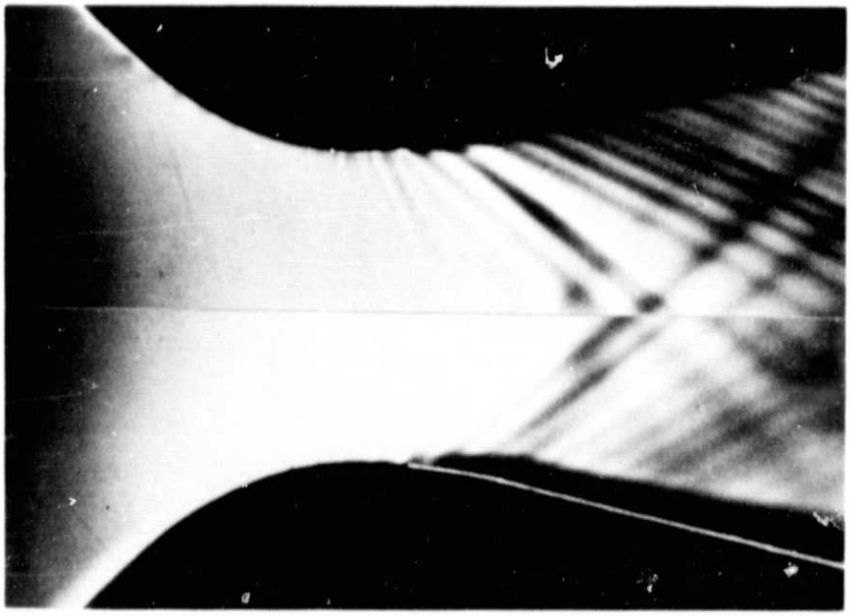

FIGURE 18 COMPOSITE PHOTOGRAPHS OF AIR FLOW IN WIND TUNNEL
UPPER HALF - WITHOUT INJECTION
LOWER HALF - WITH INJECTION OF AIR INTO AIR
(WALL DENOTED BY LIGHT LINE).

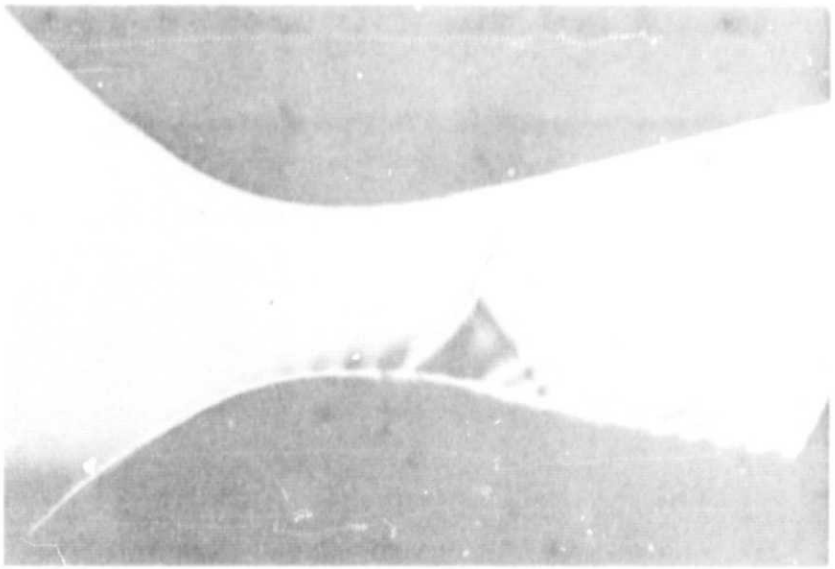

FIGURE 19a AIR FLOW WITH LOW INJECTION RATES OF FREON IN ALL THREE SECTIONS.

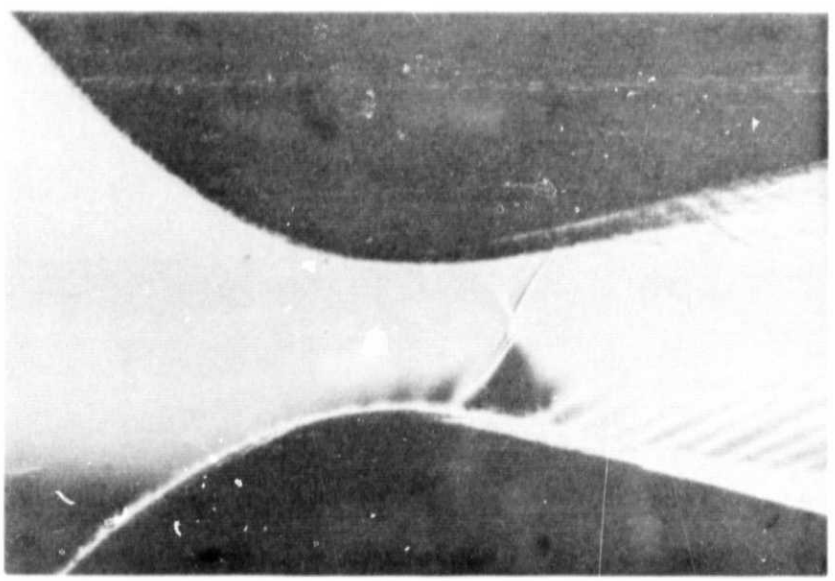

FIGURE 19b AIR FLOW WITH HIGH INJECTION RATES OF FREON IN ALL THREE SECTIONS.

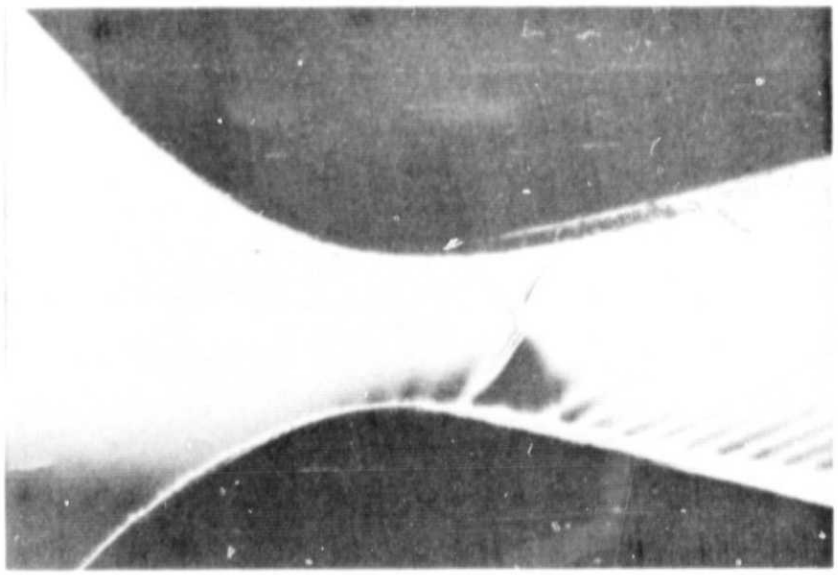

FIGURE 20a AIR FLOW WITH LOW INJECTION RATES OF CO_2 IN ALL THREE SECTIONS.

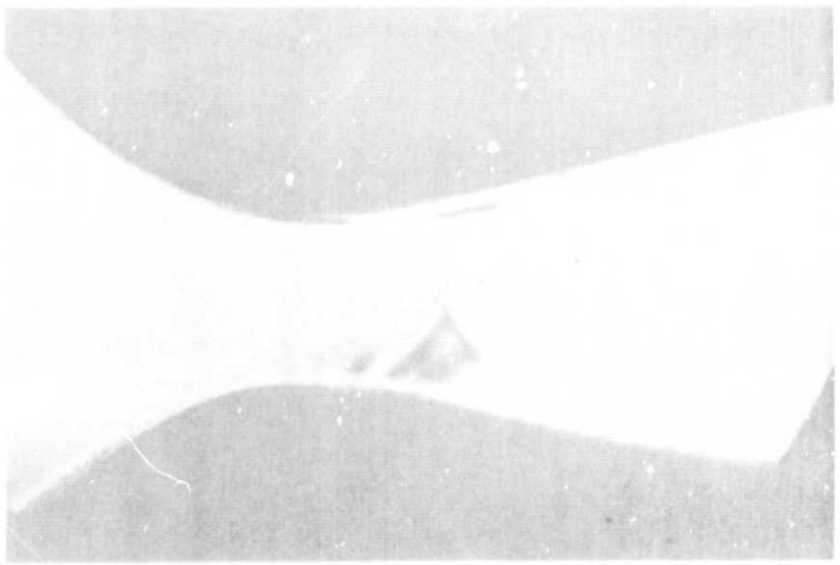

FIGURE 20b AIR FLOW WITH HIGH INJECTION RATES OF CO_2 IN ALL THREE SECTIONS.

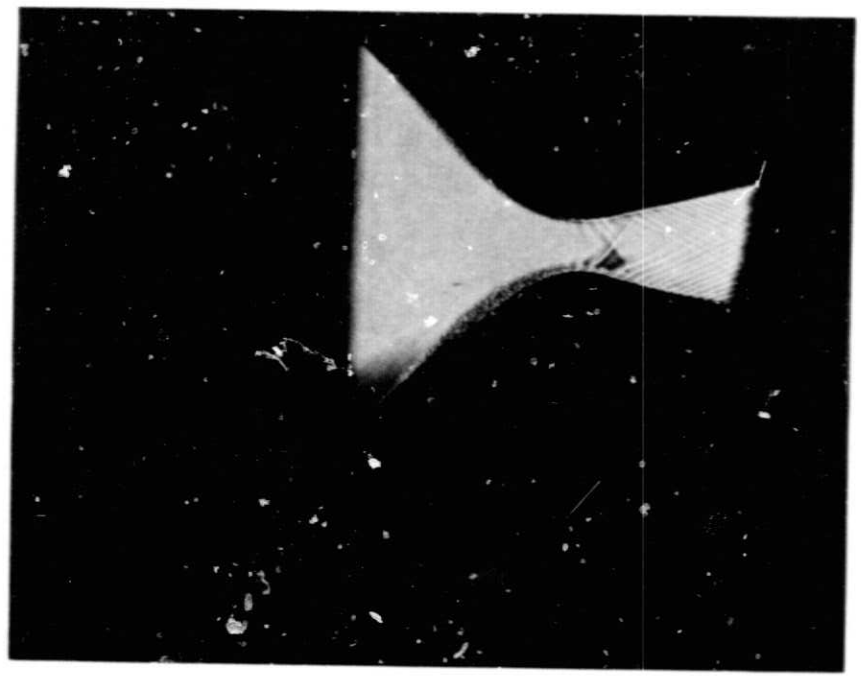

FIGURE 20c AIR FLOW WITH HIGH INJECTION RATE OF CO_2 IN FIRST SECTION ONLY.

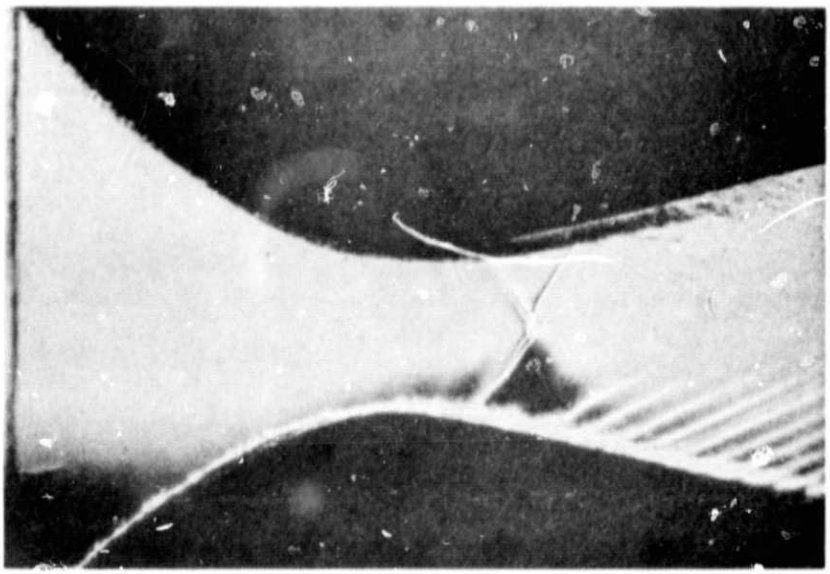

FIGURE 21a AIR FLOW WITH HIGH INJECTION RATE OF FREON IN FIRST SECTION ONLY.

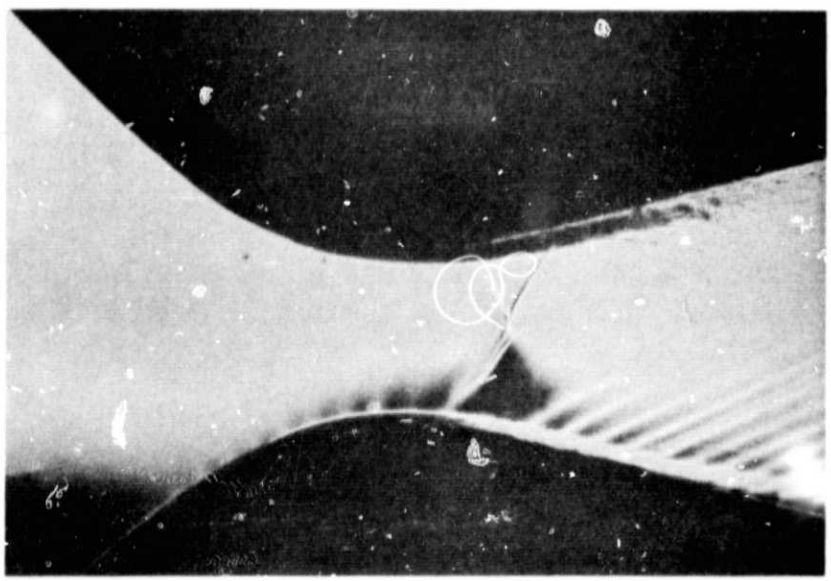

FIGURE 21b AIR FLOW WITH HIGH INJECTION RATE OF FREON IN SECOND SECTION ONLY.

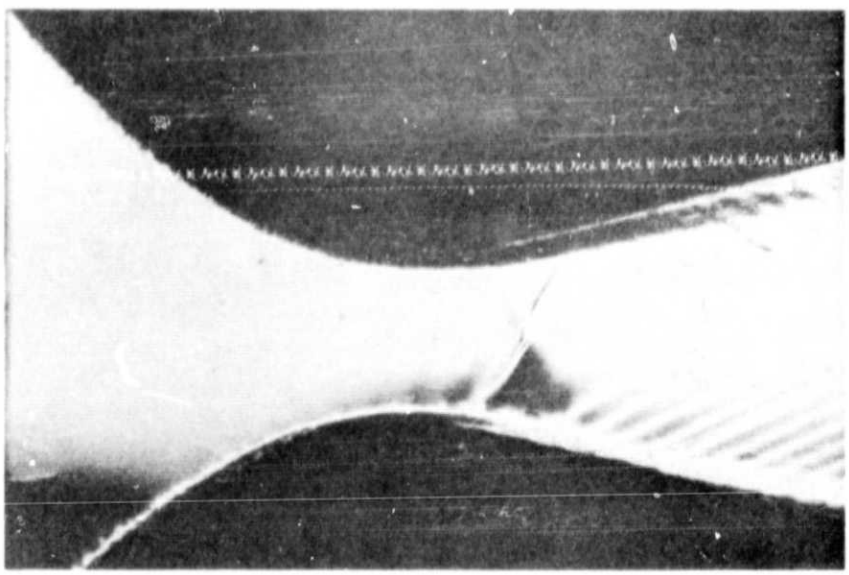

FIGURE 21c AIR FLOW WITH HIGH INJECTION RATES OF FREON IN FIRST AND SECOND SECTIONS.